From Real to Complex:Enhancing Radio-based Activity Recognition Using Complex-Valued CSI

BO WEI, Northumbria University, UK
WEN HU, University of New South Wales, Australia
MINGRUI YANG, Cleveland Clinic, US
CHUN TUNG CHOU, University of New South Wales, Australia

Activity recognition is an important component of many pervasive computing applications. Radio-based activity recognition has the advantage that it does not have the privacy concern compared with camera-based solutions, and subjects do not have to carry a device on them. It has been shown channel state information(CSI) can be used for activity recognition in a device-free setting. With the proliferation of wireless devices, it is important to understand how radio frequency interference(RFI) can impact on pervasive computing applications. In this paper, we investigate the impact of RFI on device-free CSI-based location-oriented activity recognition. We present data to show that RFI can have a significant impact on the CSI vectors. In the absence of RFI, different activities give rise to different CSI vectors that can be differentiated visually. However, in the presence of RFI, the CSI vectors become much noisier, and activity recognition also becomes harder. Our extensive experiments show that the performance may degrade significantly with RFI. We then propose a number of countermeasures to mitigate the impact of RFI and improve the performance. We are also the first to use complex-valued CSI along with the state-of-the-art Sparse Representation Classification method to enhance the performance in the environment with RFI.

CCS Concepts: • **Networks → Sensor networks**; • **Computer systems organization → Sensor networks**;

Additional Key Words and Phrases: Device-free, activity recognition, sparse representation classification, radio frequency interference , channel state information

ACM Reference Format:
Bo Wei, Wen Hu, Mingrui Yang, and Chun Tung Chou. 2010. From Real to Complex:Enhancing Radio-based Activity Recognition Using Complex-Valued CSI. *ACM Trans. Web* 9, 4, Article 39 (March 2010), 34 pages. https://doi.org/0000001.0000001

1 INTRODUCTION

Activity recognition aims to identify what a subject is doing. It is an important component of many pervasive computing applications. For example, the increasing greying population in many

Part of this research work has been published in the proceedings of the 14th International Conference on Information Processing in Sensor Networks (IPSN '15) [42]. We propose a new device-free activity recognition method using complex-valued Channel State Information (CSI) based Sparse Representation Classification method in Section 3 in this paper. The discussion regarding the evaluation on complex-valued CSI can be found in Section 4.

Authors' addresses: Bo Wei, Northumbria University, Newcastle upon Tyne, Tyne and Wear, UK, bo.wei@northumbria.ac.uk; Wen Hu, University of New South Wales, Sydney, Australia, wen.hu@unsw.edu.au; Mingrui Yang, Cleveland Clinic, Cleveland, Ohio, US, yangm@ccf.org; Chun Tung Chou, University of New South Wales, Sydney, Australia, c.t.chou@unsw.edu.au.

1559-1131/2010/3-ART39 $15.00
https://doi.org/0000001.0000001

countries puts a rising pressure on the health care system. Activity recognition can be used to improve home care for the elderlies. This paper considers the activity recognition problem using radio signals, in the device-free setting, with an emphasis on making activity recognition robust to radio frequency interference (*RFI*).

Activity recognition is a well researched topic. In terms of system components, there are three broad approaches to the activity recognition problem: camera-based [4, 7, 18, 21, 59], sensor-based [3, 6, 8, 12, 24, 48, 54] and device-free [32, 38, 41]. Cameras are able to provide high resolution data for activity recognition, but privacy is a serious concern. Although there is no privacy concern with the sensor-based approach, it imposes the requirement that a subject has to carry sensors on his body. This is inconvenient, and activity recognition fails if the subject forgets to carry the device. We have therefore chosen the device-free approach in this paper.

In the device-free approach to activity recognition, radio devices are placed in the periphery of a monitored area, called the area of interest (AoI). These radio devices send packets to each other regularly and use the received radio signal to obtain information on the radio environment. The key idea is that the radio environment is influenced by the activity taking place in the AoI. The activity recognition problem is to infer the activity from the received radio signal. In general, there are *three requirements* for the practicality of device-free activity recognition systems: *informative measurements*, *capability to deal with environment changes*, and *robustness to RFI*.

Although coarse-grained radio channel measurements, such as radio signal-strength indicators (RSSI), have been successfully used for device-free indoor localisation [43, 45, 55], they are no longer informative for activity recognition. Using informative measurements is a pre-requisite for any successful classification problem. Recent works on device-free activity recognition [32, 38, 41] have used informative Channel State Information (CSI) instead of coarse-grained radio channel measurements for activity recognition. This is also our observation, and our proposed solution, therefore, uses CSI. A challenge for CSI-based device-free activity recognition is that the CSI of the radio channel is sensitive to changes in the environment, for example new or moved furniture, due to the multi-path effect. One CSI-based activity recognition system E-eyes [41] proposed a semi-supervised approach to address the issue of environmental changes by manually updating new CSI-instances. When the system detects that the CSI-fingerprint for an activity has changed, E-eyes requires the users to label the new CSI-instances manually. A similar approach was used in [27] to deal with the impact of environmental changes on CSI-based localisation.

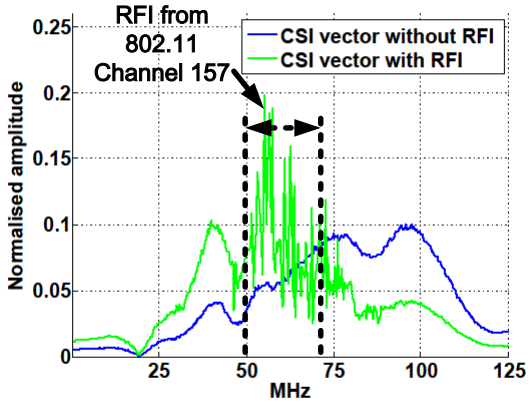

Fig. 1. CSI without and with RFI.

Another challenge for CSI-based activity recognition is that the CSI is highly influenced by RFI. The number and types of radio devices have proliferated in the last decade. It is hardly possible to find a frequency band that is clean or without RFI. Our observation, which is depicted in Fig. 1, shows that CSI is **highly impacted** by RFI[1]. The figure shows a CSI without RFI as well as a CSI with RFI in a particular radio channel. The impact of RFI on CSI is conspicuous. This implies that CSI-based activity recognition must be robust to RFI. This is the key topic of this paper. Furthermore, our proposed solution can also use the semi-supervised approach proposed by [27, 41] to update the training set and deal with the impact of environmental changes. In Section 4.10, we will show the effect of training set update for environmental changes.

As a summary of the above discussion, we have drawn a Venn diagram with the three requirements of informative measurements, robustness to environmental changes, and robustness to RFI in Fig. 2. This diagram is used to differentiate our work (indicated by a star) from two other CSI-based activity recognition solutions: E-eyes [41] and Sigg et al. [32]. It shows which solution is able to deal with which requirements. Neither of [32, 41] addresses the impact of RFI on CSI.

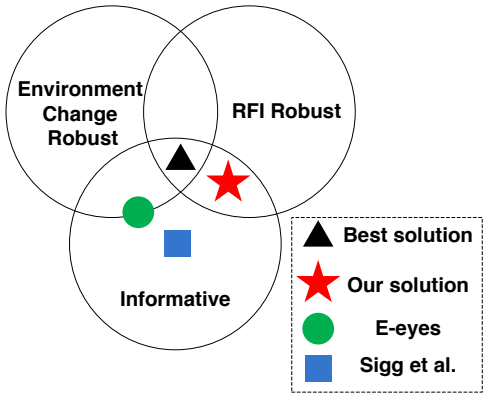

Fig. 2. Differentiating our work from other recent work on CSI-based activity recognition.

In order to enable the robustness of CSI-based location-oriented activity classification, our previous research [42] exploits the Sparse Representation Classification (SRC) approach based on ℓ_1-optimisation. SRC has been shown to be robust to noise. It has also been shown to significantly improve the classification performance in face recognition [30, 46] and acoustic classification [44], outperforming other classification approaches such as support vector machine (SVM) and k-nearest neighbours (kNN). Our previous research [42] also proposed SRC based method on the amplitudes of CSI vectors (real-valued CSI) to mitigate the influence of RFI and increases the performance of real-valued CSI based location-oriented activity recognition. In this paper, we propose a new classification method to further enhance the robustness of activity recognition using **complex-valued** CSI based SRC. Location-oriented activity recognition is able to indicate the location information as well as types of activities.

To summarise, the contributions and novelties of this paper are:

- We demonstrate by using measurements that CSI is highly impacted by RFI. We show that, while the CSI vectors for different activities in an RFI-free environment are clearly distinguishable even by naked eyes, this is no longer the case for an environment with RFI.

[1]The CSI samples in Fig. 1 are from the experiments which will be discussed in Section 4, and more details about the experiment setup can be found in Section 4.2.

- To address the above challenge, we propose a novel complex-valued CSI based SRC classification algorithm for device location-oriented activity recognition. The algorithm uses complex-valued CSI and fuses the results from a number of ℓ_1-optimisation according to their signal-to-noise ratios (SNRs). We show that this method can boost recognition accuracy and outperforms kNN and other SRC-based methods by up to 10%.
- We are also the first to propose complex-valued CSI SRC classification algorithm. Complex-valued CSI contains phase information additional to amplitude information. We show this can improve the performance compared with using only real-valued CSI.
- We study the impact of channel bandwidth on the accuracy of activity recognition. We use 4 different bandwidths: 5, 10, 15 and 20 MHz, which cover low bandwidth devices and high bandwidth devices. We show that our proposed classification algorithm produces good classification accuracy for activities with 20 MHz of bandwidth.

The rest of this paper is organised as follows. Section 2 presents background materials on CSI and SRC. We then study the impact of RFI on CSI and propose our complex-valued CSI based activity recognition method in Section 3. Next, we present evaluation results in Section 4 using experimental data collected from an apartment. Section 5 presents related work. Finally, Section 6 concludes the paper.

2 BACKGROUND

2.1 Wireless Platform and Channel State Information

We use a platform called Wireless Ad hoc System for Positioning (WASP) [25] for our experiments. The WASP nodes are originally designed for high resolution localisation and use a much wider bandwidth than many off-the-shelf wireless devices. WASP can operate in both 2.4 GHz and 5.8 GHz industrial, scientific and medical (ISM) bands, using a bandwidth of, respectively, 83 MHz and 125 MHz. WASP uses Orthogonal Frequency-Division Multiplexing (OFDM) at the physical layer and time division multiple access (TDMA) at the media access control (MAC) layer. In fact, the physical layer of WASP is implemented by using commercial off-the-shelf IEEE 802.11 radio chips.

OFDM is a multi-carrier modulation technique. At the 5.8 GHz band, the WASP nodes use 320 sub-carriers. Each of these sub-carriers has a different centre frequency. This means the received sub-carriers at two frequencies can experience different amount of phase shifts, giving different frequency response. For a sub-carrier with centre frequency f_i, the complex channel response $C(f_i)$ is related to the transmitted symbol $T(f_i)$ and received symbol $R(f_i)$ by $R(f_i) = C(f_i)T(f_i)$. The complex number $C(f_i)$ captures, respectively, the sub-carrier gain and phase shift. Let $f_1, f_2, ..., f_{320}$ denote the centre frequencies of the 320 sub-carriers that WASP nodes use. Then the CSI is a complex vector $[C(f_1), C(f_2), ..., C(f_{320})]$. More details about CSI can be found in [53]. Our previous research [42] only uses the amplitude (gain) of CSI of each sub-carrier, while in this paper complex-valued CSI is applied, which contains both the *amplitude* and *phase* shift, to improve the classification accuracy.

2.2 Sparse Representation Classification

Sparse Representation Classification (SRC) is first proposed in [46] for face recognition. It has subsequently been applied to other areas, such as acoustic classification [44] and visual tracking [16]. A key feature of SRC is its use of ℓ_1 minimisation to make the classification robust to noise. We give a brief description of SRC here, the details can be found in [46]. We assume that the classification problem has s classes. Class i is characterised by the sub-dictionary $D_i = [d_{i1}, ..., d_{in_i}]$ where d_{ij} $(j = 1, ..., n_i)$ are the n_i feature vectors derived from training data. For classification, the s sub-dictionaries are concatenated to form a dictionary $D = [D_1, D_2, ..., D_s]$. Ideally, a test sample y

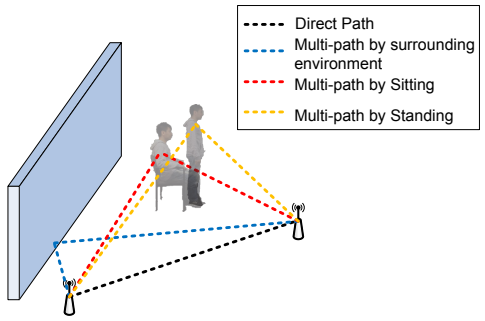

(a) Examples of multiple paths caused by different activities

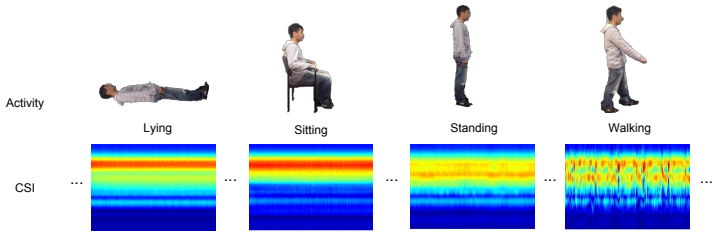

(b) Examples of CSI vectors cause by different activities (the vertical and horizontal axis are the CSI subcarries and samples)

Fig. 3. Examples of multiple paths and CSI vectors (Best view in colour)

should sit in a subspace spanned by the dictionary, i.e. there exists a *coefficient vector* x such that $y = Dx$. However, due to noise, such an x cannot be found or is perturbed. Instead, the SRC method solves for the coefficient vector x using the following ℓ_1 optimisation problem:

$$\hat{x} = \arg\min_{x} \|x\|_1 \quad \text{subject to } \|y - Dx\|_2 < \epsilon, \tag{1}$$

where ϵ is the noise level. Note that instead of requiring that $y = Dx$, the constraint requires only that the vectors y and Dx are sufficiently close to each other. The estimated coefficient vector $\hat{x}$ is used for the classification algorithm. Note that the length of $\hat{x}$ is $\sum_{i=1}^{s} n_i$. Let $\hat{x}_i$ denote the n_i-dimension sub-vector in $\hat{x}$ that corresponds to the sub-dictionary D_i. We calculate the residual $r_i = \| y - D\hat{x}_i \|_2$ for Class i. The class that gives the minimum residual is returned as the classification result. It is important to point out that ℓ_1 optimisation is also capable of handling complex-valued vectors [34, 35].

SRC has a main superiority: featureless. This provides us with an opportunity to build a training set from the CSI measurements, rather than exact feature from them. Moreover, SRC is known to be robust to noise. As our work is to study the performance of activity recognition when RFI is present, we investigate how to explore SRC to boost SNR for improving recognition performance. As far as we know, we are the first to use an SRC classification method on complex numbers.

3 ACTIVITY RECOGNITION USING COMPLEX-VALUED CSI

This section presents our method to recognise a set of location-oriented activities using CSI in the device-free setting. We first demonstrate that complex-valued CSI is influenced by activities

taking place in a room and can be used to identify location-oriented activities. We demonstrate the challenge of CSI based activity recognition when RFI is present. Finally, we present our SRC based classification method which takes RFI into consideration.

3.1 CSI contains location-oriented activity information

We first present some intuition on why device-free CSI-based location-oriented activity recognition is possible. Fig. 3(a) depicts an indoor environment with two wireless nodes and the multi-paths that the radio propagation may take. It shows that different multi-path effects can be obtained if a person is sitting or standing. It results in different CSI vectors at the receiver and can be used to identify the activity (normalised CSI amplitude vector shown in Fig. 3(b)). Furthermore, different locations of a monitored person also differentiate multi-paths, *which makes location-oriented activity recognition feasible*.

In order to demonstrate the feasibility of CSI-based activity recognition, we set up two WASP nodes in an apartment with one living room and one bedroom. The nodes are 5 metres apart with 3 walls in the line-of-sight path between the nodes. The subject is positioned in an AoI between the two nodes but is not in the direct path between the 2 nodes. The subject carries out 4 different activities: sitting, lying, standing, and walking. A WASP node is used as the transmitter and the other as a receiver. The transmitter sends to the receiver at 10 packets per seconds, and it needs a 2.5 milliseconds slot to send a packet. This means only *2.5% of running time* is occupied for sending data for activity recognition, which does not occupy bands too much to affect the radio communication of other wireless devices. For each packet received, the receiver uses the WASP interface to obtain the CSI vector and SNR for that packet. It is also important to point out that the data in this experiment are collected in a *clean* environment without any RFI.

Fig. 4(a) shows the normalised CSI amplitude vectors under the four different activities. The horizontal axis shows the sample number where a sample corresponds to a packet. There are 320 values in the vertical axis which corresponds to the 320 sub-carriers. The magnitude is shown as a heat plot. We have put four blocks of data side-by-side in the figure, which corresponds to the four activities of lying, sitting, standing and walking. It can readily be seen that the four activities have highly distinguishable CSI. This confirms that CSI contains information on activity. Another observation is that the CSI fluctuates a lot when the subject is walking. This is due to different multi-path effects created by the person walking. Fig. 4(a) shows the CSI when a 125 MHz bandwidth is used. We now show that the same observations also apply when we use a 20 MHz channel. The box in Fig. 4(a) is Channel 157 in the 802.11 standards with 20 MHz bandwidth. We have enlarged the CSI in the box and plotted it in Fig. 4(b). It can be seen that the CSI for the four activities are very distinguishable and walking creates more fluctuations in CSI.

Fig. 5(a) shows the SNR of the corresponding samples (packets). It shows that the SNR has a slightly larger fluctuation when the subject is walking. However, there does not appear to be any noticeable differences in the SNR data series among lying, sitting, and walking. These observations suggest that it may be possible to use SNR to distinguish between walking from the other three activities where the subject is stationary. However, it does not seem to be possible to use SNR to distinguish between the three stationary activities.

Since CSI is sensitive to the multi-path effect, same activity in different locations can have different CSI. Training in each interesting location must be performed for location-orientated activity recognition, and this is a limitation of CSI-based finger-printing activity recognition. Fig. 8 demonstrates the different CSI amplitudes as a result of the same activity "standing" in two locations. This fact requires additional training for same activity in different locations, but it helps location-orientated activity recognition systems locate activities. [17, 32, 41, 49, 50] also apply a similar

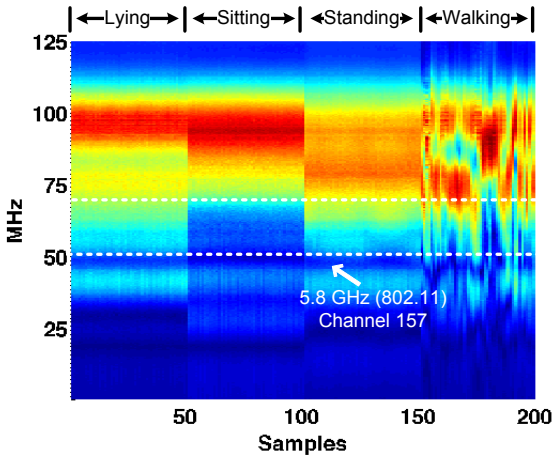

(a) CSI vectors in clean environment

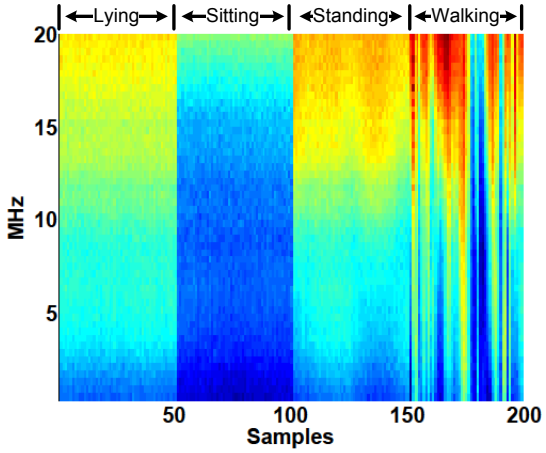

(b) CSI vectors on Channel 157 without RFI

Fig. 4. CSI performance in different activities without RFI (Best view in colour)

strategy, i.e. conducting training in various locations, for improving the performance of radio-based pattern recognition.

3.2 Challenges of CSI-based activity recognition

The results above are obtained when the two WASP nodes are in a clean environment without RFI. We conduct another experiment using the same set up, but we add a pair of IEEE 802.11a devices that communicate in Channel 157 (a 20 MHz band). Our goal is to understand the impact of RFI on CSI and SNR.

Fig. 6(a) shows the CSI for the four activities when RFI is present on Channel 157. It shows that the CSI on Channel 157 (enclosed by the white rectangle) is fairly noisy, but the four activities still have distinguishable CSI outside of Channel 157. This suggests that if wide-band devices are used to obtain the CSI for activity recognition, then we can use the part of CSI with little RFI to

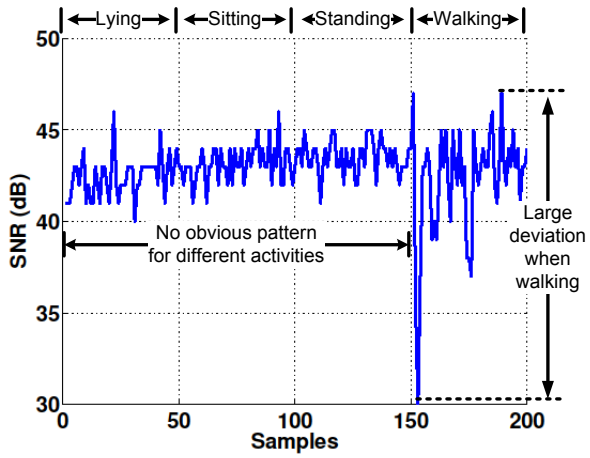

(a) SNR without RFI

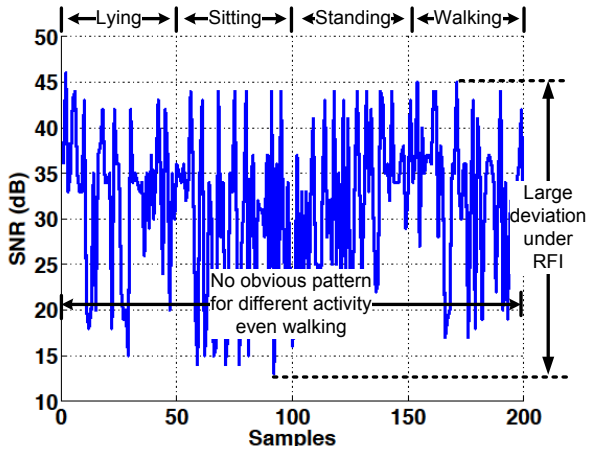

(b) SNR with RFI

Fig. 5. SNR performance in different activities

identify the activity. *However, with the ubiquitous use of wireless technologies such as WiFi, Bluetooth, IEEE 802.15.4, etc., it becomes more and more difficult or even impossible to find RFI-free bandwidth, particularly in ISM bands, for radio-based activity recognition systems. We therefore consider the possibility of using CSI in an interfered channel to perform activity recognition.*

In order to examine the effect of RFI, we plot the CSI of Channel 157 in Fig. 6(b). It shows that the CSI vectors of different activities are no longer highly distinguishable. We now examine the impact of RFI on SNR. Fig. 5(b) shows the SNR of the four activities when RFI is present on Channel 157. We see that the SNR of all four activities is highly fluctuating. We suggested earlier that it would be possible to tell walking from the static activities using SNR when RFI is absent, however, this does not appear to be feasible once RFI is present.

To further show the challenge with RFI, Fig. 7(a) and Fig. 7(b) show clusters of complex-valued CSI from the same sub-carrier with or without RFI in the complex plane. The red spots represent

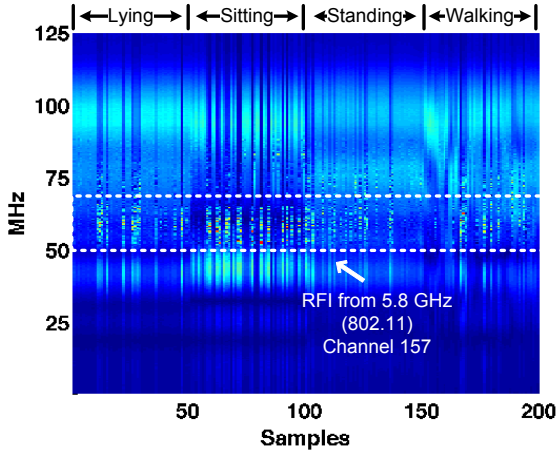

(a) CSI vectors on RFI environment

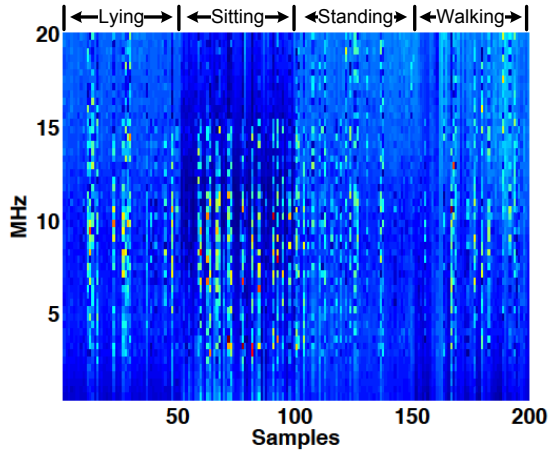

(b) CSI vectors on Channel 157 with RFI

Fig. 6. CSI performance in different activities with RFI (Best view in colour. The SNR for these samples are shown in Figure 5)

the CSI samples without RFI affected. To better show the scatter of CSI, we shift the centre to (0,0). In the clean environment without RFI, all the samples have high SNR and concentrate in a clear cluster. However, in the environment with RFI, the samples scatter in a much larger area, and less pattern can be explored compared with that in the clear environment.

However, if we look more closely at the CSI vectors of each activity, we can see that a number of CSI vectors among one activity are almost the same. This recurrence of CSI vectors suggests that we may use a block of CSI vectors for classification instead of individual CSI vectors (see Fig. 6(a) and 6(b)). However, this classification is going to be challenging because the CSI vectors appear to be fairly noisy. We will propose a few different classification methods in Section 3.3.3 to address this challenge.

To sum up, it is a challenge to use CSI to perform activity recognition when RFI is present.

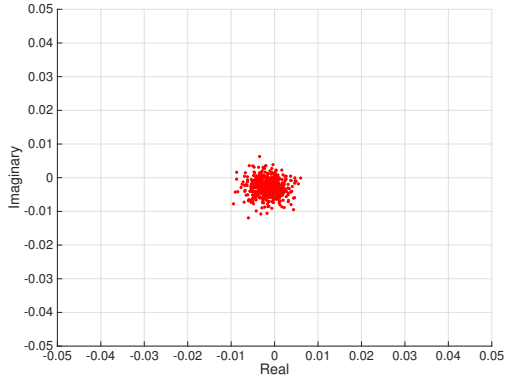

(a) a CSI subcarrier without RFI

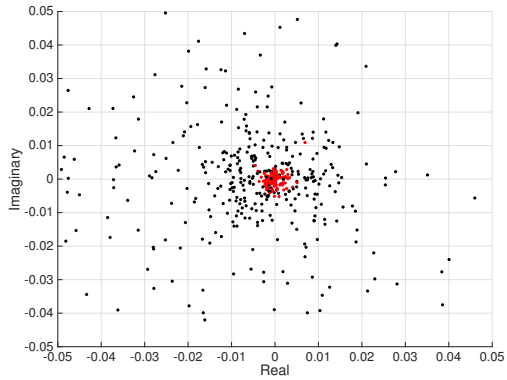

(b) a CSI subcarrier with RFI

Fig. 7. CSI performance in complex plane (Best view in colour)

3.3 Location-Oriented Activity Recognition with RFI

We now describe our proposed complex-valued CSI-based activity recognition in the presence of RFI. The goal of activity recognition is to identify four daily activities: sitting, standing, lying and walking in different rooms, as well as whether the AoI is empty.

3.3.1 Data collection. Our method fingerprints the activities using CSI complex vectors. The first procedure is to record the CSI measurements and use a CSI data sanitisation method for building a training set and use the training set to fingerprint the test data by using our proposed machine learning algorithm.

RFI causes the unexpected change to CSI vectors. There is no existing model for the performance of CSI vector under RFI. Therefore, we need to consider the RFI environment when training the dictionary. In other words, the CSI vectors of one specific activity under different physical or radio environments vary significantly. We have to update training set for a new RFI environment. The method in [41] can be applied for updating the dictionary when RFI is present.

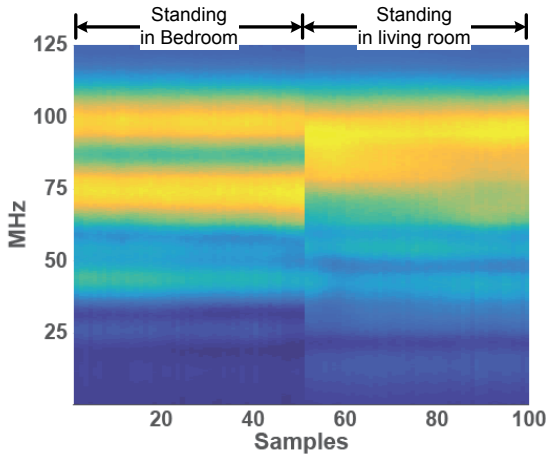

Fig. 8. CSI of standing in different locations.

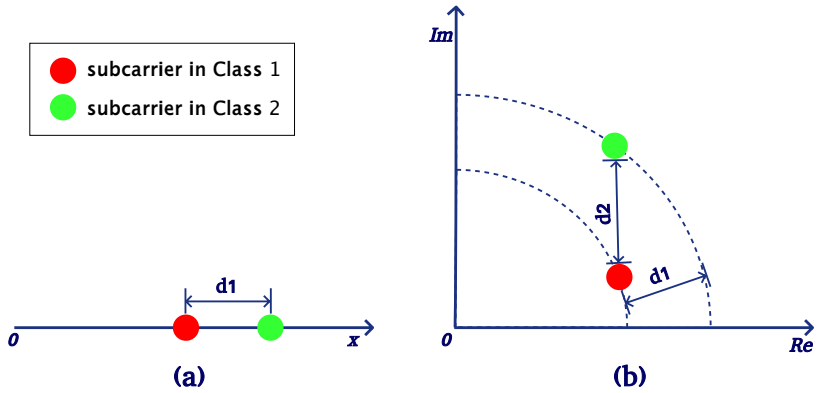

Fig. 9. Distance difference between two classes using real-valued CSI and complex-valued CSI. (a) distance using amplitude-valued CSI (b) distance using complex-valued CSI

3.3.2 CSI Data Sanitisation. We use a CSI data sanitisation method to obtain both CSI amplitude and phase information. A CSI vector with n sub-carriers, i.e. $C = [C(f_1), C(f_2), ..., C(f_n)]$. The CSI amplitude vector is the absolute values of each element. Since the receiver and transmitter do not attempt to synchronise time in OFDM and there is an unknown random phase shift in each CSI vector, a data sanitisation method to calculate the phase information is required. We use the data sanitisation method proposed in [27] for calculating this unknown phase shift. Having CSI phase information, we are ready to calculate complex-valued CSI vectors. The CSI for i-th sub-carrier is a complex number $(|\hat{C}_i| \cos(\hat{C}_i), |\hat{C}_i| \sin(\hat{C}_i))$, where $\hat{C}_i$ is the CSI complex value of i-th sub-carrier after sanitisation and $|\hat{C}_i| = |C_i|$. We apply this algorithm to all CSI vectors to remove the unknown phase shift. From now onwards, unless otherwise stated, all CSI vectors are assumed to have been sanitised.

The complex values of CSI will contain both amplitude and phase information. This is extremely important for improving performance in the environments with RFI where limited useful data can

be explored. Fig. 9 gives an intuitive explanation of this improvement. Consider the CSI of the same sub-carrier for two different classes. Fig. 9(b) depicts the situation when complex-valued CSI is used, the distance d2 between the two classes is the distance between two complex numbers on the plane. However, if only the CSI amplitudes are used, then we get the situation in Fig. 9(a) where the distance between the two classes is d1. It can be shown that d2≥d1, which means complex-valued CSI enhances the separation between different classes and therefore giving better classification performance. However, the situation is more complicated with RFI due to the multi-path effect. The phase features might introduce additional extra noise. To address this issue, classification method along with additional signal processing is explicitly required to mitigate effect from RFI and improve the recognition performance.

3.3.3 Classification algorithms. We have seen that RFI causes the CSI vector to be very noisy. In order to deal with RFI, we introduce a window size ws where ws consecutive complex-valued CSI vectors are used for classification. One possible method is to stack ws complex-valued CSI vectors into a long feature vector and use it for classification. However, this will be computationally intensive because the feature vector has a very high dimension. Instead, we will use the one complex-valued CSI vector at a time and investigate different fusion methods.

Let $y_1, y_2, ..., y_{ws}$ denote the complex-valued CSI vectors in the time window, and D be the dictionary. We first solve the following ℓ_1-optimisation problem for each complex-valued CSI vector y_i, $i = 1, .., ws$:

$$\hat{x}_i = \arg\min_x \|x\|_1 \quad \text{subject to } \|y_i - Dx\|_2 < \epsilon, \tag{2}$$

We now present three different fusion methods which use the estimated coefficients $\hat{x}_i$ ($i = 1, .., ws$) in different ways.

The first method is to use decision fusion and will be referred to as ℓ_1-*voting*. For this method, the algorithm uses each $\hat{x}_i$ to arrive at a decision class using the standard SRC algorithm described in Section 2.2. This method then uses majority voting to arrive at a decision.

The second method is to fuse the $\hat{x}_i$ vectors by computing their mean: $\hat{x}_{\text{sumup}} = \frac{1}{ws}\sum_{i=1}^{ws} \hat{x}_i$. The mean vector $\hat{x}_{\text{sumup}}$ is then used to compute the residuals for each class as in the standard SRC algorithm described in Section 2.2. This method returns the class that minimises the residual. Note that this fusion method was proposed by Misra et al. in [20] where they showed that such method could improve the GPS recovery accuracy. We will call this method ℓ_1-*sumup*.

The method ℓ_1-*sumup* applies equal weights to all $\hat{x}_i$ by computing a simple average of them. However, it is possible that some CSI vectors in the window are less affected by noise. This can also be seen from Fig. 5 where the SNR fluctuates. We therefore propose to use SNR of a sample to derive a weighting for that sample. Let S_i denote the SNR of the i-th sample in the window. We compute the weighted mean of $\hat{x}_i$ using

$$\hat{x}_{\text{weighting}} = \sum w_i \hat{x}_i, \tag{3}$$

$$w_i = \frac{A_i}{\sum_{j=1}^{ws} A_j}, \quad A_i = 10^{(\frac{S_i}{20})}, \tag{4}$$

The mean vector $\hat{x}_{\text{weighting}}$ is then used to compute the residuals for each class as in the standard SRC algorithm described in Section 2.2. This method returns the class that minimises the residual. We call this method as ℓ_1-*weighting*.

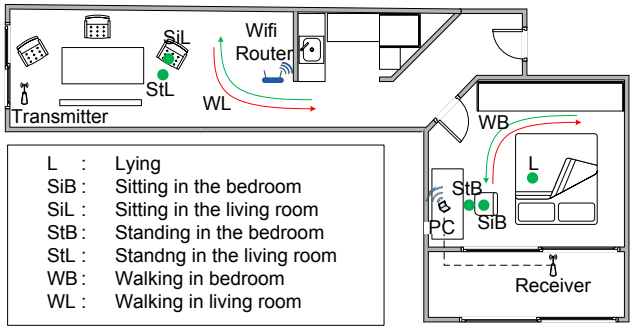

Fig. 10. Floor plan of the experiment environment

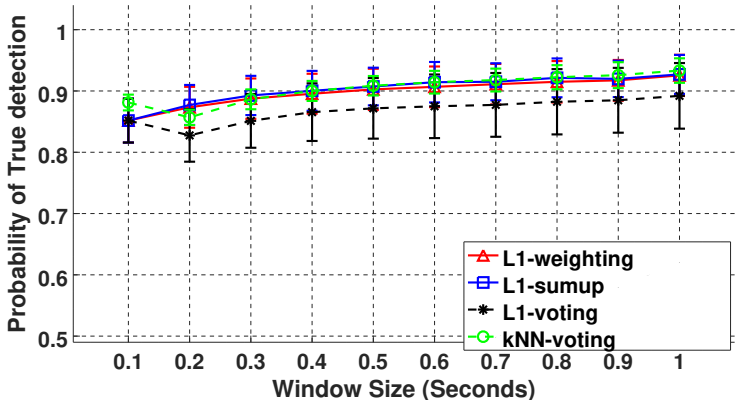

(a) "*whole bandwidth without RFI*"

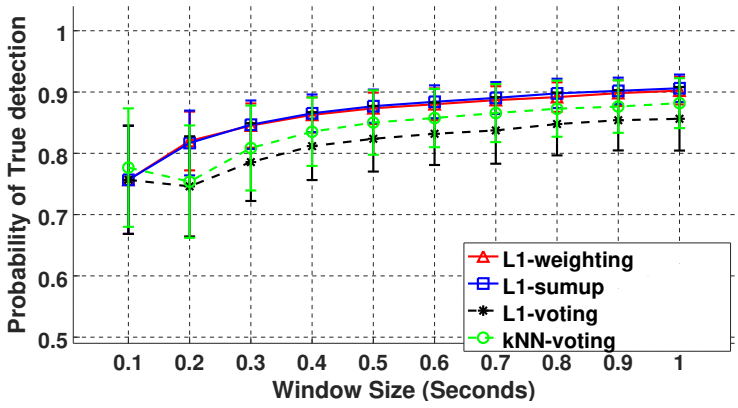

(b) "*whole bandwidth with RFI*"

Fig. 11. The Performance vs Window Size

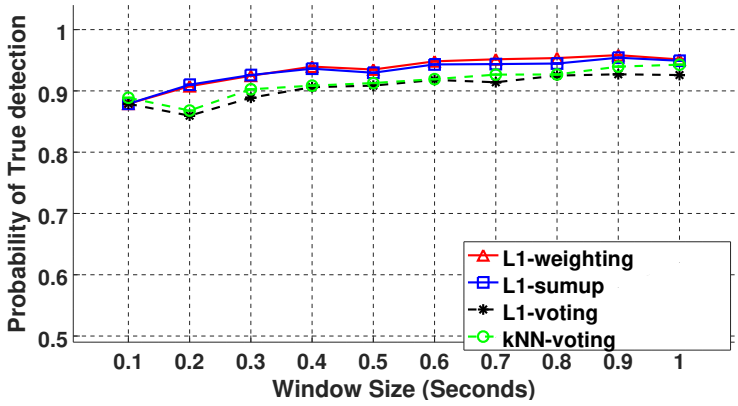

(a) "*Channel 157 without RFI*"

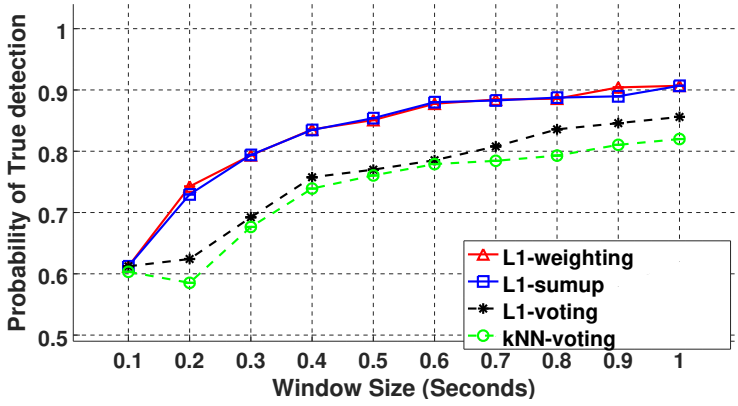

(b) "*Channel 157 with RFI*"

Fig. 12. The Performance vs Window Size

4 EVALUATION

4.1 WASP nodes

We use a pair of WASP nodes in our experimental evaluation. We provided some basic information on WASP nodes in Section 2.1. We provide further background information and explain some design choices here. We choose WASP because it is a software-defined radio and there is an API to obtain CSI. WASP can operate in both 2.4 GHz and 5.8 GHz. We choose to perform our evaluation in 5.8 GHz because this band is less used compared to the 2.4 GHz band. It is therefore easier to find places where RFI is absent across the entire 125 MHz bandwidth that WASP operates in. This allows us to do two things. First, we can experiment in a clean radio frequency (RF) environment and use CSI from the clean environment to establish benchmark for the classification algorithms. Second, this allows us to control the amount of RFI present in our experiments and we can be sure that any RFI present in the environment is added by us. We can therefore study the impact of RFI on activity recognition.

WASP is a low-power wireless platform. A pair of WASP nodes only consumes 4.5 W [25](2 W for a receiver and 2.5 W for a transmitter). WASP nodes can be powered by cable, which means the deployment of a pair of WASP nodes for activity recognition only cost no more than 4 kWh per month.

Table 1. Bandwidth for different wireless protocols

Wireless Protocol	Bandwidth per Channel	Number of Subcarrier in OFDM
2.4 GHz (802.11b/g/n)	20 MHz	52
3.6 GHz (802.11y)	5/ 10/ 20 MHz	13/ 26/ 52
4.9 GHz (802.11y)	20 MHz	52
5 GHz (802.11a)	20 MHz	52
5 GHz (802.11n)	20/ 40 MHz	52/ 104
5 GHz (802.11ac)	20/ 40/ 80 MHz	52/ 104/ 208

4.2 Experiment Setup

The experiment is conducted in an apartment whose floor plan is shown in Fig. 10. The AoI includes one living room (top half of the floor plan) and one bedroom (the room on the right). Two WASP nodes are deployed at the edge of the AoI. One node works as the transmitter and sends a beacon once every 0.1 second. This node is near the left-hand end of the apartment and is marked as transmitter in the floor plan. The other WASP node acts as a receiver, and this is where the CSI data are collected. This node is located in the balcony just outside the bedroom and marked as the receiver in the floor plan. The receiver is connected to a computer (labelled as PC in the floor plan) in the bedroom, and this computer is the sink for the CSI data. The distance between the transmitter and receiver is about 5 metres.

We consider 8 different location-oriented activity classes : (1) E: empty environment (2) L: lying on the bed in the bedroom (3) SiB: sitting in the bedroom (4) SiL: sitting in the living room (5) StB: standing in the bedroom (6) StL: standing in the living room (7) WB: walking in the bedroom (8) WL: walking in the living room. The location of the activities are marked in the floor plan in Fig. 10. We perform standing and sitting in the same location because we also want to focus on activity classification without considering different locations to evaluate the efficiency of our method. We also differentiate between sitting and standing in different locations for evaluating the location-oriented activity recognition. For each activity class, CSI data is collected for 1 minute, so that no physical environmental changes take place during this time. For a given dataset, we have 600 CSI samples for each activity, resulting in $600 \times 8 = 4,800$ CSI samples in total.

We use a computer (PC) and a WiFi router to create RFI in the environment. Their locations are marked in the floor plan in Fig. 10. They use 802.11a protocol, which operates in 5.8 GHz, to communicate on Channel 157 (a 20 MHz channel). The computer communicates with the router using the echo request `ping` command as fast as possible with the default packet size 7 kilobytes; the router responses the request with echo reply packet containing the exact data of request packet. The average transmission rate will arrive at more than 30 Mbit/s. In order to simulate the RFI that the activity recognition system may actually experience, we place the WiFi router in the middle of the apartment, which is a natural location that people will use in order to provide WiFi coverage to their apartment. The distance between the WiFi router and the receiver is about 4 metres, and the distance between the PC and the receiver is about 1.5 metres.

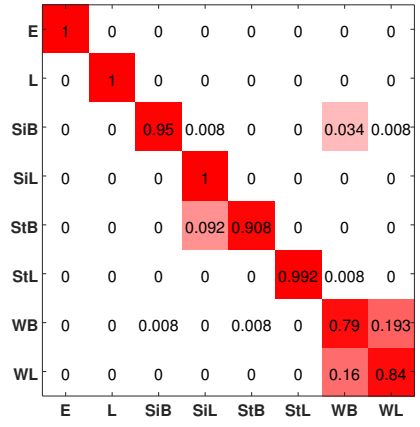

Fig. 13. Confusion matrix: $ws = 5$ and $B = 20$ MHz in "*Channel 157 without RFI*"

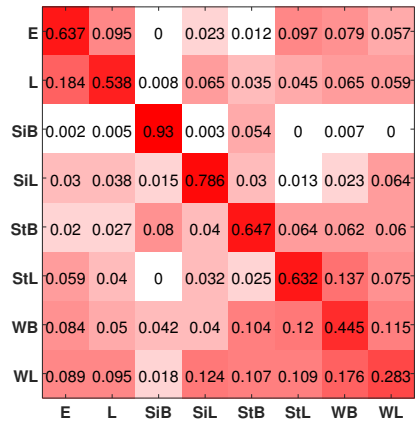

Fig. 14. Confusion matrix: $ws = 1$ and $B = 20$ MHz in "*Channel 157 with RFI*"

4.3 Evaluation methodology and metrics

We apply 10-fold cross validation to each dataset to evaluate our proposed method. We use both the probability of true detection and confusion matrix to present our results.

We have two *primary* datasets. One dataset is collected under clean environment while the other is collected when there is RFI in Channel 157. We use these datasets to investigate the effect of bandwidth on location-oriented activity recognition. In particular, we investigate what happens if we use a bandwidth of 5 MHz, 10 MHz, 15 MHz, 20 MHz, 40 MHz, 80 MHz and 125 MHz. Let us assume that we use a bandwidth window size B MHz where B is one of 5, 10, 15, 20, 40, 80 or 125. Recalling that WASP nodes have a bandwidth of 125 MHz. We first select the first B MHz of the 125 MHz-band and use the sub-carriers in the B MHz to perform classification. We then shift the bandwidth window by 5 MHz. If a *complete* B MHz can be found in the data, we perform another

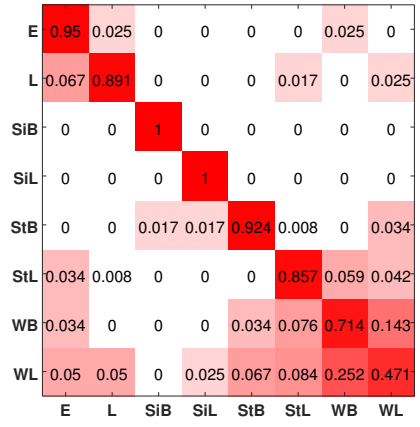

Fig. 15. Confusion matrix: $ws = 5$ and $B = 20$ MHz in "*Channel 157 with RFI*"

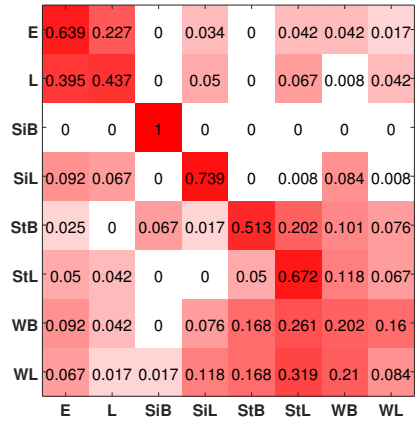

Fig. 16. Confusion matrix: $ws = 5$ and $B = 5$ MHz in "*Channel 157 with RFI*"

calculations. We iterate until the whole 125 MHz is covered. We will refer to the results obtained by sliding bandwidth window over the 125 MHz band as "*whole bandwidth without RFI*" and "*whole bandwidth with RFI*".

Instead of using the whole 125 MHz in the primary datasets. We also created two *secondary* datasets, from the with and without RFI cases, which include over those sub-carriers in Channel 157. These secondary datasets span a bandwidth of 20 MHz. Note that, when interference sources exist, all sub-carriers in the secondary datasets are with RFI while only some of the sub-carriers in the primary datasets are with RFI. By using the secondary datasets, we investigate what happens when we use a bandwidth window of 5 MHz, 10 MHz, 15 MHz, 20 MHz. The methodology of shifting the bandwidth window is the same as that for primary datasets. We will refer to the results obtained from the secondary datasets as "*Channel 157 without RFI*" and "*Channel 157 with RFI*".

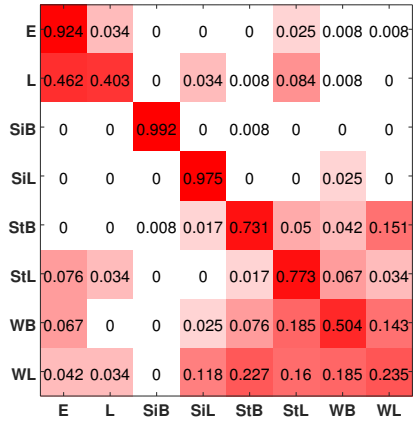

Fig. 17. Confusion matrix: $ws = 5$ and $B = 10$ MHz in "*Channel 157 with RFI*"

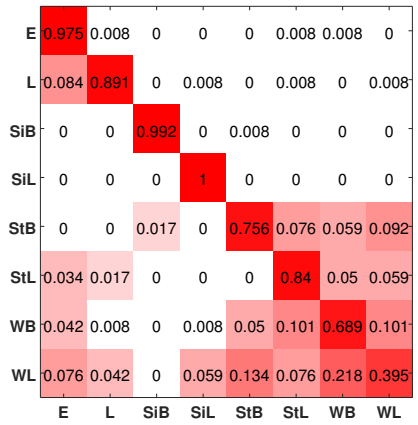

Fig. 18. Confusion matrix: $ws = 5$ and $B = 15$ MHz in "*Channel 157 with RFI*"

Our classification algorithm uses a window size of ws consecutive CSI samples for classification, as discussed in Section 2.2. We will also vary this window size in our investigation.

We consider the following 4 classification algorithms: kNN with majority voting (kNN-$voting$), ℓ_1-$voting$, ℓ_1-$sumup$ and ℓ_1-$weighting$. In order to demonstrate the improvement in using a window size ws, we also show the result of using one CSI sample or a window size of 1; we will use "kNN-$win1$" and "ℓ_1-$win1$" to denote the algorithms that use a $ws = 1$. The default SRC algorithms in this section is complex-valued unless we state otherwise. We also use complex-valued kNN for comparison.

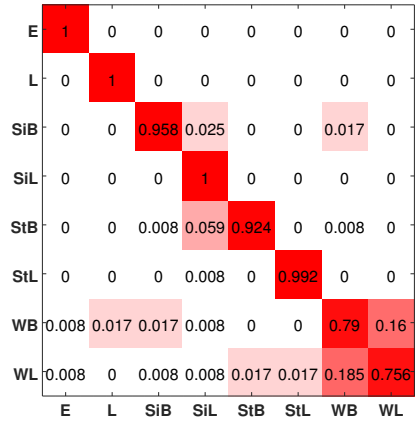

Fig. 19. Confusion matrix: Real-valued CSI, $ws = 5$ and $B = 20$ MHz in "*Channel 157 without RFI*"

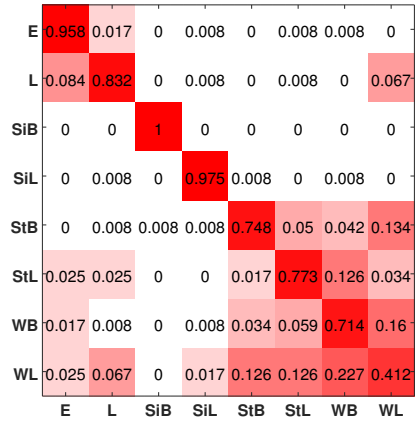

Fig. 20. Confusion matrix: Real-valued CSI, $ws = 5$ and $B = 20$ MHz in "*Channel 157 with RFI*"

4.4 Effect of Window Size

In this section, we study the impact of window size *ws* on activity recognition performance. We use *ws* from 1 to 10, which correspond to a time of 0.1 second and 1 second, because the transmitter sends beacons at a frequency of 10 Hz. We will show that window size can improve accuracy but this is at the expense of decreasing the temporal resolution of activity recognition. We will use both primary datasets ("*whole bandwidth without RFI*" and "*whole bandwidth with RFI*") and both secondary datasets ("*Channel 157 without RFI*" and "*Channel 157 with RFI*") in this study. We assume a bandwidth window size $B = 20$, which is the bandwidth of one 5.8 GHz 802.11 channel. Fig. 12 shows performance in different window size using different data fusion methods.

First, we discuss the performance of using "*whole bandwidth without RFI*". Fig. 11(a) shows the probability of true detection of the 4 different algorithms. When there is no RFI and with a 20 MHz

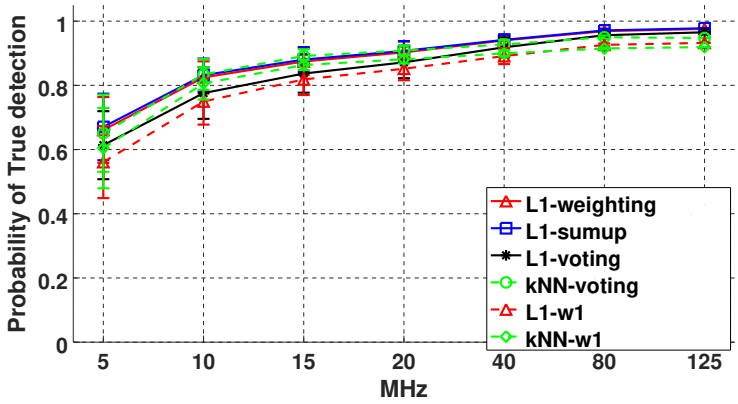

(a) "*whole bandwidth without RFI*"

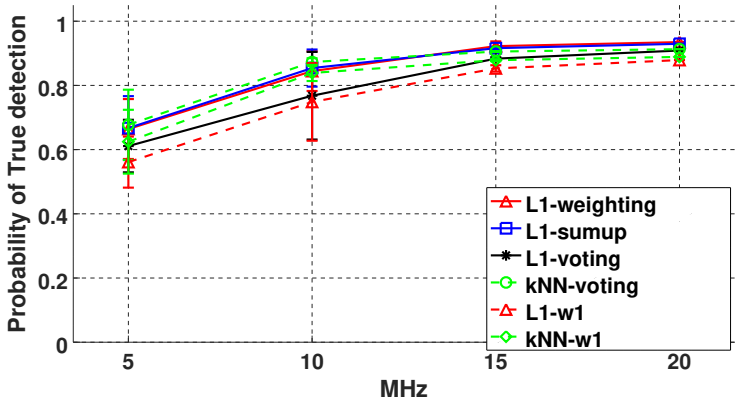

(b) "*Channel 157 without RFI*"

Fig. 21. The performance vs bandwidth window size

bandwidth window size, a window size ws of 1 can already achieve an accuracy of approximately 90% for all four classification algorithms. The accuracy gradually increases to 95% when the window size is increased to 10. The results are similar if we use "*Channel 157 without RFI*", as shown in Fig. 12(a). The algorithms ℓ_1-*weighting* and ℓ_1-*sumup* show similar performance but are slightly better than kNN−*voting* and ℓ_1-*voting*. This shows that, without RFI, very good classification accuracy can be obtained.

As we discussed earlier, the challenge is to perform classification when there is RFI. Fig. 11(b) shows the probability of true detection for the dataset "*whole bandwidth with RFI*". It shows that the performance increases with larger window size. Among the four algorithms used, ℓ_1-based algorithms outperform kNN and the best performing algorithms are ℓ_1-*weighting* and ℓ_1-*sumup*. If we compare the classification accuracy between without and with RFI in Fig. 11(a) and 11(b), we see a significant drop in accuracy when RFI is present especially when the window size is small. For example, for $ws = 1$, accuracy decreases from 85% to 76% because of RFI. We now turn to the dataset "*Channel 157 with RFI*" whose results shown in Fig. 12(b). Again,the accuracy increases when the

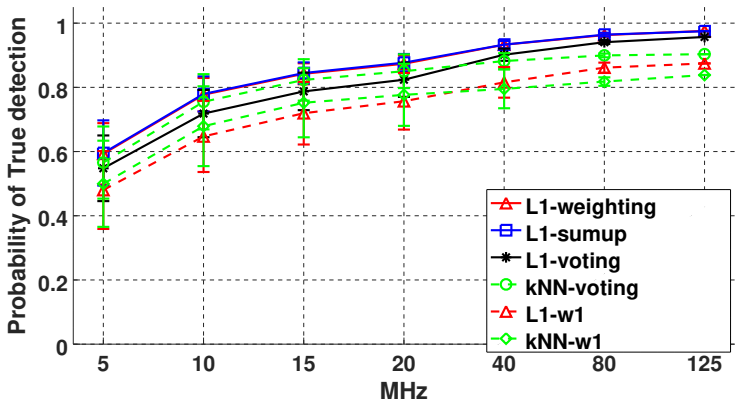

(a) "*whole bandwidth with RFI*"

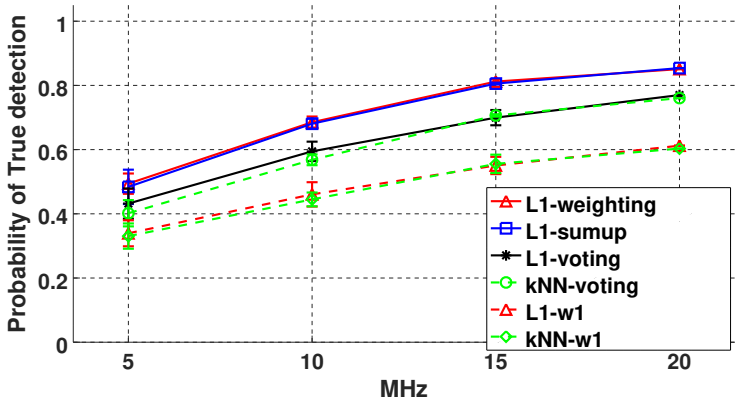

(b) "*Channel 157 with RFI*"

Fig. 22. The performance vs bandwidth window size

window size is increased, and both ℓ_1-*weighting* and ℓ_1-*sumup* perform the best. The most telling observation is that, for $ws = 1$, the classification accuracy is merely 63% but if $ws = 5$ is used, an accuracy of almost 85% can be obtained. This shows that window size can have a significant effect on performance when RFI is present.

We now present the confusion matrices for location-oriented activity recognition using our proposed ℓ_1-*weighting*. Fig. 13 shows the confusion matrix for "*Channel 157 without RFI*" with a window size of 5 (0.5 second). It shows that perfect accuracy is achieved with 5 activities. The accuracy for static activities is extremely high. The accuracy for the two walking activities are also very good. We now present the confusion matrix for "*Channel 157 with RFI*" with a window size of 0.1 second and 0.5 second, in respectively, Fig. 14 and 15. It can be seen that a big window size has significantly improved classification accuracy of many activities. In the following sections, we will use a window size $ws = 5$ (0.5 second) by default.

4.5 Effect of the Bandwidth Window Size

In this section, we discuss the influence of the bandwidth window size on the location-oriented activity recognition performance. This study takes advantage of the available wide bandwidth from WASP nodes to simulate different kinds of protocols shown in Table 1. [2]

The result of using different bandwidth window size B for dataset "*whole bandwidth without RFI*" is shown in Fig. 21(a). As expected, increasing B gives a better classification accuracy. In particular, ℓ_1-*weighting* achieves an accuracy of 70%, 90% and 95% when using a bandwidth window B of 5 MHz, 20 MHz and 125 MHz respectively. Similar trend is also observed for the dataset "*Channel 157 without RFI*" (shown in Fig. 21(b)). The algorithms ℓ_1-*weighting*, ℓ_1-*sumup*, ℓ_1-*voting* and kNN-*voting* show similar performance.

Fig. 22(a) shows the probability of true detection for the dataset "*whole bandwidth with RFI*". It shows the performance increases when the bigger bandwidth window size increases. Comparing four algorithms using window size ws 5, ℓ_1-*weighting* and ℓ_1-*sumup* perform the best, which outperform ℓ_1-*voting* and kNN-*voting*. When looking at the dataset "*Channel 157 with RFI*" (shown in Fig. 22(b)), the accuracy decreases significantly, especially when the bandwidth window sizes B are 5 MHz and 10 MHz whose accuracy decreases from 72% and 88% to 50% and 70% using ℓ_1-*weighting* compared with the dataset "*Channel 157 without RFI*". The performance of ℓ_1-*weighting* and ℓ_1-*sumup* is close, but they show their superiority over ℓ_1-*voting* and kNN-*voting*, for example, the accuracy of ℓ_1-*weighting* and ℓ_1-*sumup* is 5% better than ℓ_1-*voting* and kNN-*voting* when the bandwidth window size B is 20 MHz. This shows ℓ_1-*weighting* and ℓ_1-*sumup* algorithms increase the recognition performance when there is RFI.

Fig. 16, Fig. 17, Fig. 18 and Fig. 15 illustrate the confusion matrix using ℓ_1-*weighting* with the bandwidth window size B 5 MHz, 10 MHz, 15 MHz and 20 MHz respectively in the dataset "*Channel 157 with RFI*". It shows that the using larger bandwidth window size B helps increase the accuracy and robustness to RFI. When the bandwidth window size B is 20 MHz, 2 static activities have perfect accuracy, 2 static activities have accuracy more than 90%, the other 2 static activities have accuracy more than 85%, and "walking in bedroom" has the accuracy more than 70%.

4.6 Effect of Different Distances Between the Router and Receiver

In order to evaluate the impact of the amount of interference on classification. We vary the distance between one interferer (the WiFi router in the floor plan in Fig. 10) and the WASP receiver. We consider 4 cases: no interference (NONE), interferer just next to the the receiver (0mR), 0.5 metre away from the receiver (0.5mR), and 1 metre away form the receiver (1mR). The classification uses only Channel 157. The computer also communicates with the router using the echo request `ping` command as fast as possible.

Fig. 23 shows the influence of receiver-interferer distance on the probability of true detection. It shows that for 0mR, the accuracy can drop by more than 10%. However, by using a window size $ws = 5$, ℓ_1-*weighting* has an accuracy about 60%. Note that there is not much difference between the 0.5mR and 1mR cases. Also, there is only a slight drop in performance for the ℓ_1 algorithms between NONE and 0.5mR cases. This shows that if an interferer is not present within 0.5m of the receiver, then the activity recognition accuracy is still high.

[2] Since our radio-based activity recognition system uses CSI information from Physical layer, the feasibility of using other protocols for the same purpose is also subject to the availability of CSI from their drivers. When their drivers are able to provide CSI, it is expected that they can achieve the similar performance discussed in Section 4.5.

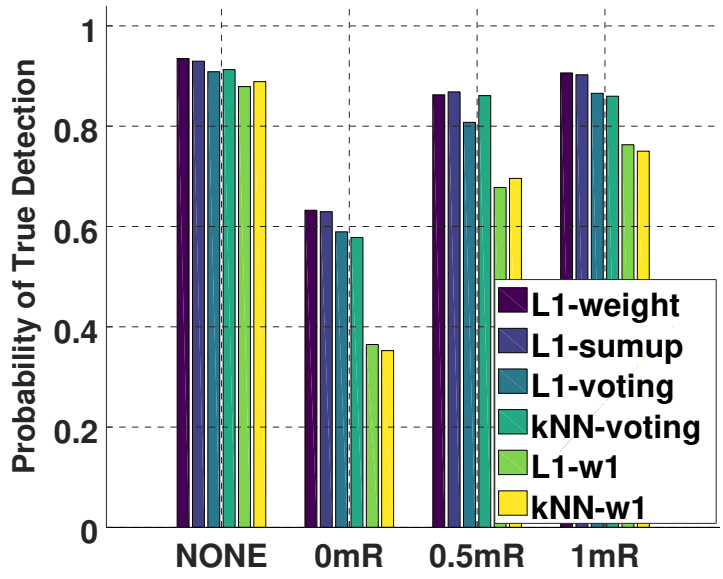

Fig. 23. The performance influenced by the distances between the router and the receiver

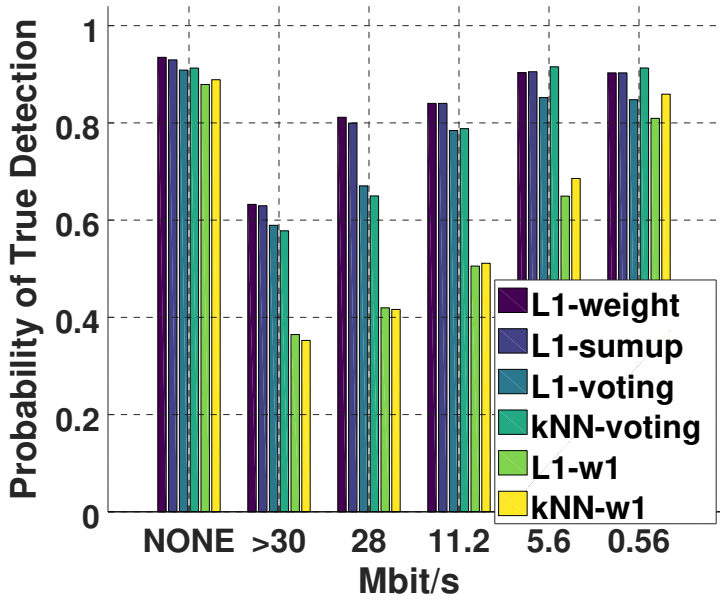

Fig. 24. The performance under different transmission rates between the router and the receiver

Table 2. Features for SNR based walking detection

Feature	Equation
Standard Deviation	$\sigma = \frac{1}{n-1}\sqrt{E[(S(k)-\mu)^2]}$
Peak	$\rho = max(S) - min(S)$
Head Size	$\eta = max(S) - median(S)$
3rd Order Central moment	$\gamma = E[(S(k)-\mu)^3]$

4.7 Effect of Different traffic Between Interference Source and Receiver

In this section, we study the effect of traffic sending rates on the classification performance. We keep one interference source (the WiFi router in the floor plan in Fig. 10) next to the receiver and adjust the `ping` rates of the interferer. The `ping` rate is set to "as fast as possible" (average transmission rate more than 30 Mbit/s), 500 packets per second (transmission rate 28 Mbit/s), 200 packets per second(transmission rate 11.2 Mbit/s), 100 packets per second (transmission rate 5.6 Mbit/s) and 10 packets per second (transmission rate 0.56 Mbit/s). These settings roughly correspond to the bit rates of watching online videos with frame rates 1080p, 480p and 360p, which give rise to bit rates of 8 Mbit/s, 5 Mbit/s and 1 Mbit/s respectively.

Fig. 24 shows the classification performance under different transmission rates. Our proposed ℓ_1-*weighting* method reaches 80% accuracy when transmission rate is 28 Mbit/s, which means it is robust to the transmission rate 28 Mbit/s. In contrast, the accuracy of both ℓ_1-*voting* and kNN-*voting* algorithm is no more than 70%. *This means our proposed ℓ_1-weighting is more robust to RFI than the other methods.* Moreover, ℓ_1-*weighting* achieves an accuracy of 85% when the transmission rate is 11.2 Mbit/s. The accuracy stays almost the same for lower transmission rates.

4.8 SNR based Walking Detection Discussion

In Section 3, we discuss the possibility of using SNR to differentiate walking from non-walking, i.e. a detection or binary classification problem. We see from Fig. 5(a) that, when RFI is absent, this is probably feasible because walking gives rise to highly fluctuating RSS while non-walking does not. However, in the presence of RFI, the distinction between walking and non-walking is not so conspicuous, as seen in Fig. 5(b). In this section, we want to investigate what classification performance we can get if we use SNR for walking detection. This study is also motivated by the fact that many device-free localisation methods [9, 60, 61] use SNR as a feature to find the location of the person in AoI.

The detection problem is to detect whether the person is walking. This covers the classes of WL and WB instead of walking detection with location information. A commonly used feature for device-free localisation is the variance of the SNR, which is used in for example [60]. However, in order to minimise the possibility that walking detection fails due to poor choice of features, we have chosen to use 4 different features listed in Table 2: Standard Deviation, Peak, Head Size, and 3rd Order Central moment where S is SNR vectors and μ is the mean of SNR values in a vector. For training, we use a logistic regression model.

The alternative to using SNR for walking detection is to use CSI with ℓ_1 classifier. We will compare these two methods. The comparison uses 10-fold cross validation and measurements from Channel 157. We consider two datasets, "*Channel 157 without RFI*" and "*Channel 157 with RFI*". Also, for both datasets, we use bandwidth window sizes B of 5 MHz, 10 MHz and 20 MHz bands.

Since walking detection is binary classification, we use the following metrics:

- **True Positive Rate (TPR)**: $TPR = TP/(TP + FN)$
- **False Positive Rate (FPR)**: $FPR = FP/(FP + TN)$

Table 3. Performance of walking detection (Better statistics in each column is highlighted)

	Without RFI			With RFI		
Bandwidth	5 MHz	10 MHz	20 MHz	5 MHz	10 MHz	20 MHz
TPR (SNR)	**0.7059**	**0.8740**	0.9076	0.0924	0.1975	0.4370
FPR (SNR)	0.0420	**0.0187**	**0.0070**	**0.0256**	**0.0490**	0.0506
F1 score (SNR)	**0.7648**	**0.9052**	0.9407	0.1446	0.2885	0.5428
TPR (CSI)	0.4706	0.8313	**0.9913**	**0.3277**	**0.5336**	**0.8393**
FPR (CSI)	**0.0056**	0.112	0.0084	0.0938	0.0574	**0.0309**
F1 score (CSI)	0.6328	0.8314	**0.9833**	**0.4073**	**0.6256**	**0.8393**

Table 4. True Detection Rates using complex-valued CSI vs Real CSI: "Channel 157 without RFI"

	L1_weight	L1_sumup	L1_voting	L1_w1	kNN_voting	kNN_w1
Complex	0.935	0.930	0.909	0.879	0.913	0.889
Real	0.928	0.929	0.888	0.856	0.912	0.885

Table 5. True Detection Rates using complex-valued CSI vs Real CSI: "Channel 157 with RFI"

	L1_weight	L1_sumup	L1_voting	L1_w1	kNN_voting	kNN_w1
Complex	0.851	0.854	0.770	0.612	0.760	0.603
Real	0.801	0.807	0.752	0.558	0.748	0.575

- **F1 score**: $F1\ score = 2TP/(2TP + FP + FN)$

where TP, TN, FP and FN are the number of true positives, true negatives, false positives, and false negatives respectively.

Table 3 shows the comparison between detection using SNR and using CSI. Each column illustrates one bandwidth window size B in each dataset and we highlight the better statistics. A number of observations can be made: (1) In the absence of RFI, detection using SNR has a higher TPR compared to using CSI for a bandwidth window of 5 MHz and 10 MHz; however, for a bandwidth window of 20 MHz, detection using CSI has a higher TPR. (2) In the absence of RFI, it is viable to use either SNR or CSI based detector for walking detection. (3) RFI causes the performance of both detectors to decrease. However, the SNR-based detector has a sharper drop in TPR. (4) Overall, the CSI-based detector is more robust in the presence of RFI.

4.9 Effect on Complex-valued CSI

4.9.1 Effect of Complex-Valued CSI Based Classification Discussion. In this section, we explore the advantage of complex-valued CSI based classification. As illustrated in Fig. 9, complex-valued CSI can enlarge the separation between classes. To further support this, we calculate the distances *between* and *within* classes. We use the metric, which was introduced to calculate the distance between two classes and tune SVM hyperparameters [33]. The distance is defined as

$$D(C_1, C_2) = \frac{2}{n_1 n_2} \sum_{i=1}^{n_1} \sum_{j=1}^{n_2} d\left(\frac{x_{1,i}}{||x_{1,i}||}, \frac{x_{2,i}}{||x_{2,i}||}\right) - \frac{1}{n_1^2} \sum_{i=1}^{n_1} \sum_{j=1}^{n_1} d\left(\frac{x_{1,i}}{||x_{1,i}||}, \frac{x_{1,j}}{||x_{1,j}||}\right) - \frac{1}{n_2^2} \sum_{i=1}^{n_2} \sum_{j=1}^{n_2} d\left(\frac{x_{2,i}}{||x_{2,i}||}, \frac{x_{2,j}}{||x_{2,j}||}\right) \quad (5)$$

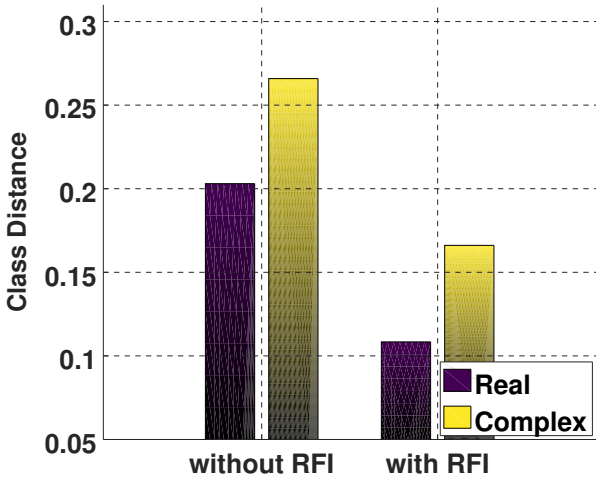

Fig. 25. Class difference in "Channel 157 without RTI" and "Channel 157 with RTI"

, where C_1 and C_2 are samples for two classes, n_1 and n_2 are the numbers of samples in each class. $x_{k,i}$ is the i-th sample in Class k. The function d calculates the Euclidean distance between two vectors. This metric considers distances between two classes as well as the distance within each class. We average distances between each pair of classes to calculate *class distance*. The longer class distance will help improve the classification performance as a result.

Fig. 25 shows the *class distances* by using real-valued CSI and complex-valued CSI. In the dataset "*Channel 157 without RTI*", the class distance is 0.203 using real-valued CSI. The class distance rises 31.0% to 0.266 when using complex-valued CSI. The class distance decreases to 0.108 when using real-valued CSI in the dataset "*Channel 157 with RTI*" due to the existence of RFI. When using the complex-valued, the class distance significantly rises 52.0% to 0.166. There are two observations: (1) RFI can reduce the class distance, which results in the reduction of the recognition performance. (2) Complex-valued CSI can increase the class distance significantly, and improve the classification results in return.

We will further confirm this using the true detection rates. Table 4 shows the true detection rates in the dataset "*Channel 157 without RTI*". The accuracy stays similar without RFI when using complex-valued and real-valued based CSI. When looking at the dataset "*Channel 157 with RTI*", the accuracy improves significantly using complex-valued CSI. Table 5 shows the true detection rates in the dataset "*Channel 157 without RTI*". When using complex-valued CSI, the true detection rate of ℓ_1-*win*1 increases from 55.8% to 61.2%. Applying data fusion methods, real-valued CSI based ℓ_1-*weighting*, ℓ_1-*sumup* and ℓ_1-*voting* can achieve 80.1%, 80.7% and 75.2% respectively. When using complex-valued CSI, their accuracy increases to 85.1%, 85.4% and 77.0%. This shows the complex-valued CSI can help improve recognition performance with RFI. Fig. 13, Fig. 15, Fig. 19 and Fig. 20 demonstrate the confusion matrices of these settings using ℓ_1-*weighting*, which also confirms the fact that complex-valued CSI achieves better recognition performance. Complex-valued CSI can supply phase information additional to amplitude information. When the environment is without RFI, the amplitude information is capable of showing clear distinguishable patterns, so the performance stays similar in the dataset "*Channel 157 without RTI*". However, the additional phase

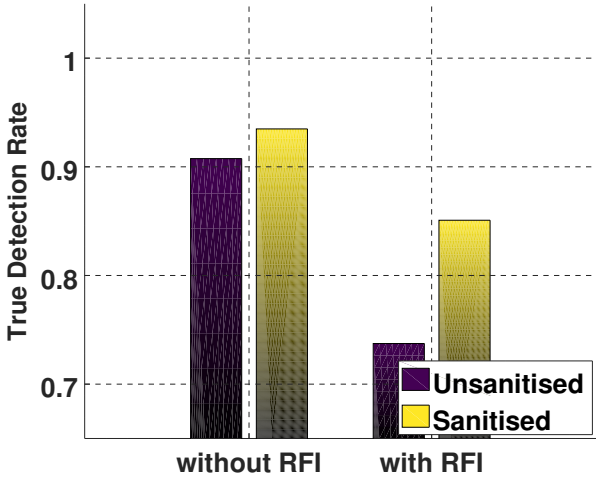

Fig. 26. The comparison between sanitised and unsanitised complex-valued CSI in "Channel 157 without RTI" and "Channel 157 with RTI"

information is important for the scenario with RFI and helps improve the recognition accuracy, where CSI amplitude is not sufficiently informative.

4.9.2 Effect of Sanitised CSI . To show the effect of Sanitised CSI, we also use the default setting. For unsanitised CSI, we directly use the raw CSI vectors without any sanitisation. Fig. 26 shows the true detection rates using sanitised and unsanitised CSI. In the dataset "*Channel 157 without RFI*", the accuracy increases from 90.76% to 93.48%. When introducing RFI in the dataset "*Channel 157 with RFI*", the accuracy drops to 73.73% with unsanitised CSI. After sanitising, the accuracy increases to 85.08%. This shows it can significantly improve performance using sanitised CSI.

4.9.3 Effect of Complex-valued SRC . In this section, we discuss the effect of SRC using complex-valued CSI. We are the first to apply complex-valued ℓ_1 minimisation for classification tasks. To compare with complex-valued SRC, we combine phase vectors and amplitude vectors into one column as inputs (*"Features in Column"*) for a real-valued SRC. Figure 27 shows the true detection using in the dataset "*Channel 157 with RFI*" and "*Channel 157 without RFI*". In the dataset "*Channel 157 without RFI*", the accuracy slightly increases from 93.17% to 93.48%. With RFI in the dataset "*Channel 157 with RFI*", the accuracy decreases to 85.08% using our proposed method, while the true detection rate is only 80.36% using *"Features in Column"* method.

4.10 The effect of dictionary update for environmental changes

In this section, we show the effect of dictionary update for environment changes. It is known that CSI is extremely sensitive to environmental changes due to the multi-path effect. When the environment changes, we use a similar strategy in [27, 41] that updates the dictionary and conduct activity recognition. Figure 28 shows the performance of our proposed methods in two environments with different furniture deployment. We use the default dataset "*Channel 157 with RFI*" as "*Environment 1*". We change the furniture deployment and collect the CSI measurements when the activities are performed in the same place with RFI in Channel 157 for the dataset "*Environment 2*". Evaluating our methods on "*Environment 2*", we update and build the dictionary using newly

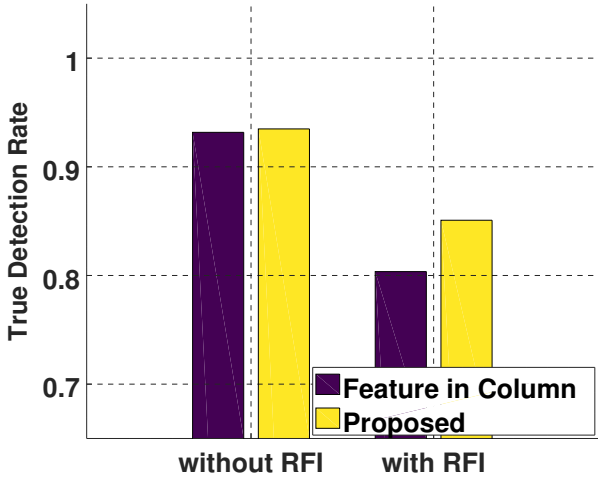

Fig. 27. The comparison between sanitised complex-valued CSI and CSI features in one column in "Channel 157 without RTI" and "Channel 157 with RTI"

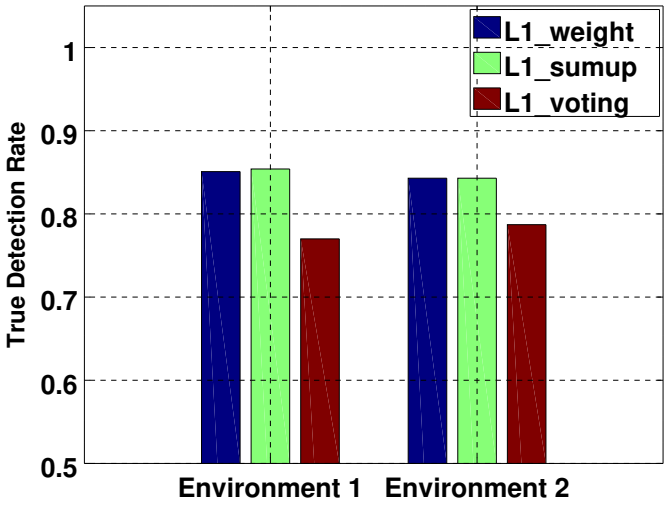

Fig. 28. The comparison of the performance in two environments

collected CSI measurements for activity recognition. As shown in Figure 28, the performance of our proposed methods are equivalent in "*Environment 1*" and "*Environment 2*". ℓ_1-*sumup* achieves 85.08% and 84.29%, and ℓ_1-*weight* achieves 85.40% and 84.29% in "*Environment 1*" and "*Environment 2*", which both outperform ℓ_1-*voting* with the true detection rates 76.99% and 78.71% in these two

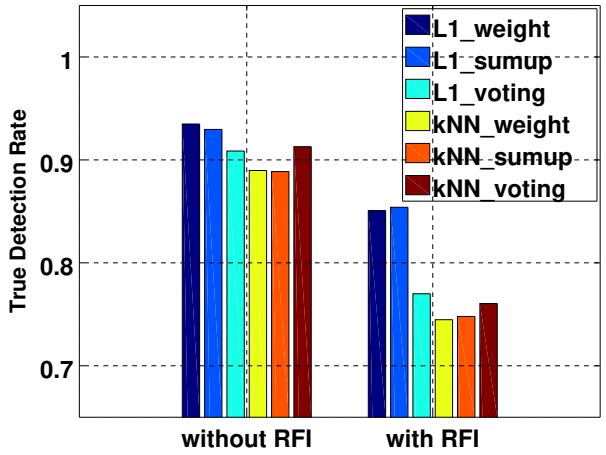

Fig. 29. The comparison among fusion methods using ℓ_1 and kNN in "Channel 157 without RTI" and "Channel 157 with RTI"

environments, respectively. This confirms that our proposed methods are capable to deal with environmental changes by updating the dictionary and work in practice.

4.11 Comparison with fusion methods using kNN

In this section, we compare with ℓ_1 based fusion methods with kNN based fusion methods. For fair comparison, we introduce similar strategies of ℓ_1-*sumup* and ℓ_1-*weight* to kNN based data fusion methods. The same as Section 3.3.3, we denote $y_1, y_2, ..., y_{ws}$ as the complex-valued CSI vectors in the time window, and D as the dictionary. We first calculate distance vectors z between one complex-valued CSI vector and each sample in the dictionary D. For a complex-valued CSI vector y_i, $z_{ij} = \|y_i - D_j\|_2$, where z_{ij} is the jth element for the distance vector z_i and the length of z_i is the number of samples in D. The first data fusion method kNN-*sumup* is to fuse z_i by computing their mean within a window ws, $\hat{z}_{\text{sumup}} = \frac{1}{ws}\sum_{i=1}^{ws} z_i$. The second method kNN-*weight* is to fuse z_i by additionally considering SNR of a sample, $\hat{z}_{\text{weighting}} = \frac{1}{ws}\sum_{i=1}^{ws}(z_i/S_i)$, where S_i is SNR of the ith sample. We select k nearest neighbours according to the distance vector $\hat{z}_{\text{sumup}}$ or $\hat{z}_{\text{weighting}}$, and vote to arrive at a decision. Figure. 29 shows the performance of both ℓ_1 and kNN based data fusion methods in "Channel 157 without RTI" and "Channel 157 with RTI". kNN voting is the normal kNN without any data fusion. It conspicuously shows that ℓ_1 based fusion methods still outperform kNN based data fusion methods. When only looking at kNN based data fusion methods, the normal kNN performs better than the data fusion based methods kNN-*sumup* and kNN-*weight*. This implies that data fusion introduces extra noise to kNN distance vectors when considering all samples within a window. This again confirms that traditional classification methods are not sufficiently robust to noise even along with explicit data fusion methods.

5 RELATED WORK

We have already discussed the most related work, i.e. work on using CSI for activity classification, in Section 1. In this section, we discuss work in activity recognition, pattern recognition from radio data and the application of compressed sensing on wireless sensor networks.

5.1 Activity recognition

Activity recognition forms the basis of many context aware pervasive computing applications. We can broadly classify activity recognition according to whether they are sensor-based or camera-based. Many sensor-based activity recognition systems have been proposed. Acceleration sensor is one of the most frequently used sensors [3, 12, 24]. This is because miniature acceleration sensors are cheap and readily available, and they can be found on all smartphones. For example, Keally et al. [10] used sensors smartphone as well as sensors wore on wrists, ankles and head to distinguish between walking, cycling, sitting and other activities. Recently, a number of wristbands, that are equipped with acceleration sensor, are available in the market. Products such as Jawbone Up [8] and Xiaomi Mi Band [48] can achieve good activity recognition accuracy but they require the users to wear the devices.

Microphone is another sensor that has been used in activity recognition. Hao et al. [6] present a method to monitor sleep quality using microphone; however, it is not sure whether the same method will function in daily activity recognition in a noisy environment. Yatani and Truong [54] design a wearable acoustic sensor which can be used to record the sound near the throat of the user, and use the measurements for activity recognition. Again, the issue is that the subject has to wear a sensor.

Cameras are also widely used for activity recognition, localisation and tracking [4, 7, 13, 18, 21, 28, 59]. An advantage of camera sensors is that they free the subjects the need to wear or to remember to wear a device. Another advantage is that they provide very rich data which can be used to distinguish between many different activities. However, the Achilles' heel of using camera for activity recognition is privacy concern. Also, cameras can only cover a limited area. For monitoring in an apartment, a camera is needed in each room. On the contrary, activity recognition using radio signals can cover a much wider area and can "see" through walls, while cameras cannot. We have therefore chosen to use device-free radio-based activity recognition which does not need subjects to carry a device and has no privacy concerns.

Visible light is also used for human sensing. Li et. al. [14] developed a testbed using off-the-shelf LED for both human sensing and communication.

5.2 Radio based pattern recognition

The propagation of radio waves in an environment is affected by the objects and people in the environment, through reflection, diffraction, constructive and destructive interference and so on. There is much interest in using the received signal characteristics to infer about the attributes of people and objects in an environment. The received signal characteristics used can be coarse or fine grained.

An example of coarse grained radio signal feature is RSSI which measures the received signal power. RSSI has been successfully used in device-free localisation [9, 43, 45, 51, 60, 61]. This is because a person standing in an area between the transmitter and receiver can attenuate, reflect, scatter the radio waves. These effects create a characteristic pattern in RSSI which can be used to infer the location of people in the environment.

Unfortunately, only limited information on the environment can be inferred from RSSI. There is a growing interest to use fine grained features of radio signals for inference. This is also fuelled by the availability of API to query CSI from WiFi chipsets such as Intel 5300 [5] and Atheros 9390 [26]. CSI has been used for many pattern recognition problems, including localisation [27], human detection [63], activity recognition [32, 41], fine-grained gesture recognition [17] , "lip-read" [36], emotion recognition [58], identity recognition[37, 56, 57] and smoking detection[62].

Some research works also use phase information for radio based device-free applications [15, 23, 39, 40], but they either use conventional classification methods or see phase as additional and independent information. As mentioned in Section 1, our work differs from earlier work on integrating complex-valued CSI into the SRC method for activity recognition in that we take RFI into consideration while earlier work did not. Among them, Ma et.al. [15] show the feasibility of using 20 MHz radio band to recognise 276 gestures, which means our proposed system has the ability of recognising much more types of activities. In our proposed system, we conduct recognition for the most common activities in the living environment and instead focus on mitigating RFI.

Radio signals have also been used to perform gesture recognition. WiSee designed by Adib et al. [2] and WiVi designed by Pu et al. [22] used software-defined radio to extract the Doppler effect caused by the gesture. In order to reduce energy consumption, Kellogg et al. [11] built AllSee which uses RFID tags and power-harvesting sensors for gesture recognition. However, these works can only recognise dynamic gestures and are not able to detect static activities because they rely on Doppler effect. To further improve the resolution of the radio signal based localisation and gesture recognition, Adib et al. [1] design WiTrack and obtain time-of-flight from the Frequency Modulated Carrier Wave (FMCW) technology for localisation in 3 dimensions. Witrack has high resolution for localisation (approximately 10 cm) but needs to use a bandwidth of 1.69 GHz. However, we show in this paper as few as 20 MHz of bandwidth can be used to distinguish static activities with good accuracy. Moreover, none of these works design their systems with RFI, while our work takes RFI into consideration.

5.3 Application of Compressed Sensing on Wireless Sensor Networks

Recently, compressed sensing has been applied to wireless sensor networks. SRC proposed by Wright et al. [46] is one of the applications of compressed sensing which helps increase the recognition performance. Wei et al. [44] developed an acoustic classification method on wireless sensor networks by applying SRC to increase the recognition performance and decrease the computation time to meet the requirement of real-time classification. Shen et al. [30, 31] optimised the SRC to boost the face recognition performance in smartphones.

Besides recognition, compressed sensing is also applied to background subtraction [28, 29, 52], data compression for in-situ soil moisture sensing [47], and cross-correlation for acoustic ranging [19] and GPS ranging [20].

Compared with these works, this paper is the first to investigate the feasibility of SRC for radio-based activity recognition. Furthermore, our work also takes advantage of SRC for activity recognition with RFI in present.

6 CONCLUSION

In this paper, we investigate the performance of radio based device-free location-oriented activity recognition systems under RFI using complex-valued CSI and propose a novel fusion algorithm based on SRC that can improve the recognition performance of the systems by up to 10% when RFI is present. Our prototype robust location-oriented activity recognition system requires only one pair of nodes for a one-bedroom apartment, which enables easy system set-up and maintenance.

REFERENCES

[1] Fadel Adib, Zach Kabelac, Dina Katabi, and Robert C. Miller. 2014. 3D Tracking via Body Radio Reflections. In *NSDI '14*. Seattle, WA.

[2] Fadel Adib and Dina Katabi. 2013. See Through Walls with WiFi!. In *SIGCOMM '13*. ACM, New York, NY, USA, 75–86.

[3] Ling Bao and Stephen S Intille. 2004. Activity recognition from user-annotated acceleration data. In *Pervasive computing*. Springer, 1–17.

[4] Isaac Cohen and Hongxia Li. 2003. Inference of human postures by classification of 3D human body shape. In *AMFG 2003*. IEEE, 74–81.

[5] Daniel Halperin, Wenjun Hu, Anmol Sheth, and David Wetherall. 2011. Tool Release: Gathering 802.11n Traces with Channel State Information. *ACM SIGCOMM CCR* 41, 1 (Jan. 2011), 53.

[6] Tian Hao, Guoliang Xing, and Gang Zhou. 2013. iSleep: unobtrusive sleep quality monitoring using smartphones. In *SenSys*. ACM, 4:1–4:14.

[7] Michael Harville and Dalong Li. 2004. Fast, integrated person tracking and activity recognition with plan-view templates from a single stereo camera. In *CVPR 2004.*, Vol. 2. IEEE, II–398.

[8] Jawbone. 2014. UP. https://jawbone.com/up. (2014). [Online; accessed 28-Agust-2014].

[9] Ossi Kaltiokallio, Maurizio Bocca, and Neal Patwari. 2012. Enhancing the accuracy of radio tomographic imaging using channel diversity. In *IEEE MASS 2012*. IEEE, 254–262.

[10] Matthew Keally, Gang Zhou, Guoliang Xing, Jianxin Wu, and Andrew Pyles. 2011. PBN: towards practical activity recognition using smartphone-based body sensor networks. In *SenSys*. ACM, 246–259.

[11] Bryce Kellogg, Vamsi Talla, and Shyamnath Gollakota. 2014. Bringing Gesture Recognition to All Devices. In *NSDI 14*. USENIX, Seattle, WA.

[12] Jennifer R Kwapisz, Gary M Weiss, and Samuel A Moore. 2011. Activity recognition using cell phone accelerometers. *ACM SigKDD Explorations Newsletter* 12, 2 (2011), 74–82.

[13] Leap Motion Inc. 2014. Leap Motion. https://www.leapmotion.com/. (2014). [Online; accessed 15-September-2014].

[14] Tianxing Li, Chuankai An, Zhao Tian, Andrew T Campbell, and Xia Zhou. 2015. Human sensing using visible light communication. In *Proceedings of the 21st Annual International Conference on Mobile Computing and Networking*. ACM, 331–344.

[15] Yongsen Ma, Gang Zhou, Shuangquan Wang, Hongyang Zhao, and Woosub Jung. 2018. SignFi: Sign Language Recognition Using WiFi. *Ubicomp 2018* 2, 1 (2018), 23.

[16] Xue Mei and Haibin Ling. 2011. Robust visual tracking and vehicle classification via sparse representation. *IEEE TPAMI* 33, 11 (2011), 2259–2272.

[17] Pedro Melgarejo, Xinyu Zhang, Parameswaran Ramanathan, and David Chu. 2014. Leveraging Directional Antenna Capabilities for Fine-grained Gesture Recognition. In *UbiComp '14*. ACM, New York, NY, USA, 541–551. DOI: http://dx.doi.org/10.1145/2632048.2632095

[18] Microsoft. 2014. Kinect. http://www.microsoft.com/en-us/kinectforwindows/. (2014). [Online; accessed 28-Agust-2014].

[19] Prasant Misra, Wen Hu, Mingrui Yang, and Sanjay Jha. 2012. Efficient Cross-correlation via Sparse Representation in Sensor Networks. In *IPSN 2012*. ACM, New York, NY, USA, 13–24. DOI: http://dx.doi.org/10.1145/2185677.2185680

[20] Prasant Kumar Misra, Wen Hu, Yuzhe Jin, Jie Liu, Amanda Souza de Paula, Niklas Wirstrom, and Thiemo Voigt. 2014. Energy efficient GPS acquisition with sparse-GPS. In *IPSN 2014*. IEEE Press, 155–166.

[21] Nuria Oliver, Eric Horvitz, and Ashutosh Garg. 2002. Layered representations for human activity recognition. In *ICMI 2002*. IEEE, 3–8.

[22] Qifan Pu, Sidhant Gupta, Shyamnath Gollakota, and Shwetak Patel. 2013. Whole-home gesture recognition using wireless signals. In *MobiCom 2013*. 27–38.

[23] Kun Qian, Chenshu Wu, Zimu Zhou, Yue Zheng, Zheng Yang, and Yunhao Liu. 2017. Inferring motion direction using commodity wi-fi for interactive exergames. In *CHI 2017*. ACM, 1961–1972.

[24] Nishkam Ravi, Nikhil Dandekar, Preetham Mysore, and Michael L Littman. 2005. Activity recognition from accelerometer data. In *AAAI*, Vol. 5. 1541–1546.

[25] Thuraiappah Sathyan, David Humphrey, and Mark Hedley. 2011. WASP: A system and algorithms for accurate radio localization using low-cost hardware. *Systems, Man, and Cybernetics, Part C: Applications and Reviews, IEEE Transactions on* 41, 2 (2011), 211–222.

[26] Souvik Sen, Jeongkeun Lee, Kyu-Han Kim, and Paul Congdon. 2013. Avoiding multipath to revive inbuilding wifi localization. In *MobiSys 2013*. ACM, 249–262.

[27] Souvik Sen, Božidar Radunovic, Romit Roy Choudhury, and Tom Minka. 2012. You are facing the Mona Lisa: spot localization using PHY layer information. In *MobiSys 2012*. ACM, 183–196.

[28] Yiran Shen, Wen Hu, Junbin Liu, Mingrui Yang, Bo Wei, and Chun Tung Chou. 2012. Efficient Background Subtraction for Real-time Tracking in Embedded Camera Networks. In *SenSys '12*. ACM, New York, NY, USA, 295–308. DOI: http://dx.doi.org/10.1145/2426656.2426686

[29] Yiran Shen, Wen Hu, Mingrui Yang, Junbin Liu, Bo Wei, Simon Lucey, and Chun Tung Chou. 2016. Real-time and robust compressive background subtraction for embedded camera networks. *IEEE Transactions on Mobile Computing* 15, 2 (2016), 406–418.

[30] Yiran Shen, Wen Hu, Mingrui Yang, Bo Wei, Simon Lucey, and Chun Tung Chou. 2014. Face Recognition on Smartphones via Optimised Sparse Representation Classification. In *IPSN '14*. IEEE Press, Piscataway, NJ, USA, 237–248. http://dl.acm.org/citation.cfm?id=2602339.2602366

[31] Yiran Shen, Mingrui Yang, Bo Wei, Chun Tung Chou, and Wen Hu. 2017. Learn to recognise: exploring priors of sparse face recognition on smartphones. *IEEE Transactions on Mobile Computing* 16, 6 (2017), 1705–1717.

[32] Stephan Sigg, Markus Scholz, Shuyu Shi, Yusheng Ji, and Michael Beigl. 2014. RF-sensing of activities from non-cooperative subjects in device-free recognition systems using ambient and local signals. *IEEE TMC* 13, 4 (2014), 907–920.

[33] Jiancheng Sun, Chongxun Zheng, Xiaohe Li, and Yatong Zhou. 2010. Analysis of the distance between two classes for tuning SVM hyperparameters. *IEEE transactions on neural networks* 21, 2 (2010), 305–318.

[34] Ewout Van Den Berg and Michael P Friedlander. 2008. Probing the Pareto frontier for basis pursuit solutions. *SIAM Journal on Scientific Computing* 31, 2 (2008), 890–912.

[35] Ewout Van den Berg and Michael P Friedlander. 2011. Sparse optimization with least-squares constraints. *SIAM Journal on Optimization* 21, 4 (2011), 1201–1229.

[36] Guanhua Wang, Yongpan Zou, Zimu Zhou, Kaishun Wu, and Lionel M Ni. 2014. We can hear you with Wi-Fi!. In *MobiCom 2014*. ACM, 593–604.

[37] Wei Wang, Alex X Liu, and Muhammad Shahzad. 2016. Gait recognition using wifi signals. In *Proceedings of the 2016 ACM International Joint Conference on Pervasive and Ubiquitous Computing*. ACM, 363–373.

[38] Wei Wang, Alex X Liu, Muhammad Shahzad, Kang Ling, and Sanglu Lu. 2017. Device-Free Human Activity Recognition Using Commercial WiFi Devices. *IEEE Journal on Selected Areas in Communications* 35, 5 (2017), 1118–1131.

[39] Xuyu Wang, Lingjun Gao, Shiwen Mao, and Santosh Pandey. 2017. CSI-based fingerprinting for indoor localization: A deep learning approach. *IEEE TVT* 66, 1 (2017), 763–776.

[40] Xuyu Wang, Chao Yang, and Shiwen Mao. 2017. PhaseBeat: Exploiting CSI phase data for vital sign monitoring with commodity WiFi devices. In *ICDCS*. IEEE, 1230–1239.

[41] Yan Wang, Jian Liu, Yingying Chen, Marco Gruteser, Jie Yang, and Hongbo Liu. 2014. E-eyes: device-free location-oriented activity identification using fine-grained WiFi signatures. In *MobiCom 2014*. ACM, 617–628.

[42] Bo Wei, Wen Hu, Mingrui Yang, and Chun Tung Chou. 2015. Radio-based device-free activity recognition with radio frequency interference. In *Proceedings of the 14th International Conference on Information Processing in Sensor Networks*. ACM, 154–165.

[43] Bo Wei, Ambuj Varshney, Neal Patwari, Wen Hu, Thiemo Voigt, Chou, and Chun Tung. 2015. dRTI: Directional Radio Tomography. In *IPSN '15*. ACM, Seattle, WA, USA, 12.

[44] Bo Wei, Mingrui Yang, Yiran Shen, Rajib Rana, Chun Tung Chou, and Wen Hu. 2013. Real-time classification via sparse representation in acoustic sensor networks. In *SenSys 2013*. ACM, 21.

[45] J. Wilson and N. Patwari. 2010. Radio Tomographic Imaging with Wireless Networks. *IEEE TMC* 9, 5 (2010), 621–632. DOI: http://dx.doi.org/10.1109/TMC.2009.174

[46] J Wright, A.Y. Yang, A Ganesh, S.S. Sastry, and Y. Ma. 2009. face recognition via sparse representation. *TPAMI* 31, 2 (2009), 210–227.

[47] Xiaopei Wu and Mingyan Liu. 2012. In-situ Soil Moisture Sensing: Measurement Scheduling and Estimation Using Compressive Sensing. In *IPSN '12*. ACM, New York, NY, USA, 1–12. DOI: http://dx.doi.org/10.1145/2185677.2185679

[48] Xiaomi. 2014. Mi Band. http://www.mi.com/shouhuan. (2014). [Online; accessed 28-August-2014].

[49] Chenren Xu, Bernhard Firner, Robert S. Moore, Yanyong Zhang, Wade Trappe, Richard Howard, Feixiong Zhang, and Ning An. 2013. SCPL: Indoor Device-free Multi-subject Counting and Localization Using Radio Signal Strength. In *IPSN '13*. ACM, New York, NY, USA, 79–90. DOI: http://dx.doi.org/10.1145/2461381.2461394

[50] Chenren Xu, Bernhard Firner, Yanyong Zhang, Richard Howard, Jun Li, and Xiaodong Lin. 2012. Improving RF-based Device-free Passive Localization in Cluttered Indoor Environments Through Probabilistic Classification Methods. In *IPSN '12*. ACM, New York, NY, USA, 209–220. DOI: http://dx.doi.org/10.1145/2185677.2185734

[51] Chenren Xu, Mingchen Gao, Bernhard Firner, Yanyong Zhang, Richard Howard, and Jun Li. 2012. Towards Robust Device-Free Passive Localization Through Automatic Camera-Assisted Recalibration. In *ACM SenSys*.

[52] Weitao Xu, Yiran Shen, Neil Bergmann, and Wen Hu. 2016. Sensor-assisted face recognition system on smart glass via multi-view sparse representation classification. In *Proceedings of the 15th International Conference on Information Processing in Sensor Networks*. IEEE Press, 2.

[53] Zheng Yang, Zimu Zhou, and Yunhao Liu. 2013. From RSSI to CSI: Indoor Localization via Channel Response. *ACM Comput. Surv.* 46, 2, Article 25 (Dec. 2013), 32 pages. DOI: http://dx.doi.org/10.1145/2543581.2543592

[54] Koji Yatani and Khai N Truong. 2012. Bodyscope: a wearable acoustic sensor for activity recognition. In *Ubicomp 2012*. ACM, 341–350.

[55] Moustafa Youssef, Matthew Mah, and Ashok Agrawala. 2007. Challenges: device-free passive localization for wireless environments. In *MobiCom 2007*. ACM, 222–229.

[56] Yunze Zeng, Parth H Pathak, and Prasant Mohapatra. 2016. WiWho: wifi-based person identification in smart spaces. In *Proceedings of the 15th International Conference on Information Processing in Sensor Networks*. IEEE Press, 4.

[57] Jin Zhang, Bo Wei, Wen Hu, and Salil S Kanhere. 2016. Wifi-id: Human identification using wifi signal. In *Distributed Computing in Sensor Systems (DCOSS), 2016 International Conference on*. IEEE, 75–82.

[58] Mingmin Zhao, Fadel Adib, and Dina Katabi. 2016. Emotion recognition using wireless signals. In *Proceedings of the 22nd Annual International Conference on Mobile Computing and Networking*. ACM, 95–108.

[59] Tao Zhao, Manoj Aggarwal, Rakesh Kumar, and Harpreet Sawhney. 2005. Real-time wide area multi-camera stereo tracking. In *CVPR 2005*, Vol. 1. IEEE, 976–983.

[60] Yang Zhao and N. Patwari. 2011. Noise reduction for variance-based device-free localization and tracking. In *SECON 2011*. 179–187. DOI: http://dx.doi.org/10.1109/SAHCN.2011.5984895

[61] Yang Zhao, Neal Patwari, Jeff M. Phillips, and Suresh Venkatasubramanian. 2013. Radio Tomographic Imaging and Tracking of Stationary and Moving People via Kernel Distance. In *IPSN '13*. ACM, New York, NY, USA, 229–240. DOI: http://dx.doi.org/10.1145/2461381.2461410

[62] Xiaolong Zheng, Jiliang Wang, Longfei Shangguan, Zimu Zhou, and Yunhao Liu. 2017. Design and implementation of a CSI-based ubiquitous smoking detection system. *IEEE/ACM Transactions on Networking* 25, 6 (2017), 3781–3793.

[63] Zimu Zhou, Zheng Yang, Chenshu Wu, Longfei Shangguan, and Yunhao Liu. 2013. Omnidirectional Coverage for Device-free Passive Human Detection. *IEEE TPDS* (2013).

Received February 2007; revised March 2009; accepted June 2009